ACS OMEGA

http://pubs.acs.org/journal/acsodf

Article

Atmospheric-Pressurized Process for Dimethyl Carbonate/Methanol Separation with and without Heat Integration: Design and Control

Hong-mei Wei, Fu-jie Wang, Hong-wei Yan, Wei-Zhou Jiao,* and Wei Wei*

Cite This: *ACS Omega* 2023, 8, 20450−20470

Read Online

ACCESS | Metrics & More | Article Recommendations | Supporting Information

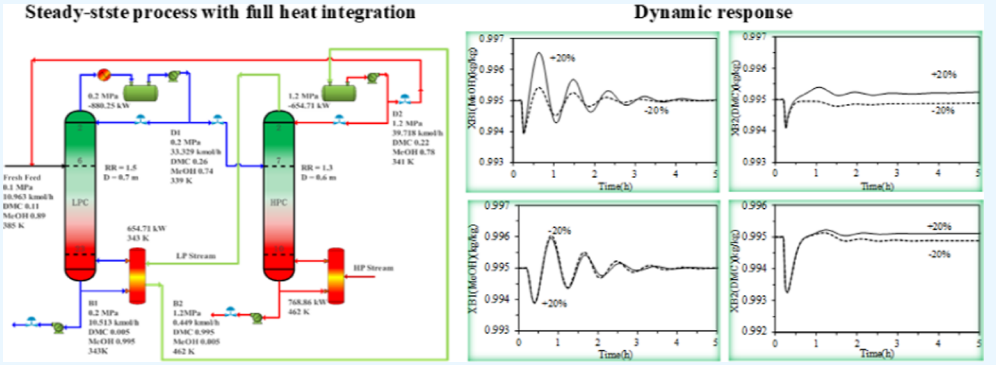

ABSTRACT: Process economy and dynamic controllability are critical for DMC/MeOH separation via the PSD process. In this paper, rigorous steady-state and dynamic simulations of atmospheric-pressurized process for DMC/MeOH separation with no, partial, and full heat integration have been carried out with Aspen Plus and Aspen Dynamics. Further investigations have been conducted into the economic design and dynamic controllability of the three neat systems. Simulation results indicated that: the separation process via full and partial heat integration provided TAC savings of 39.2 and 36.2%, respectively, compared to that of no heat integration; the non-heat-integrated system displays good dynamic performance, critical dynamic penalties were demonstrated for both partial and full heat integration processes, while the partial one exhibited a more robust control except for precisely maintaining X_{B2}(DMC); a PCTC scheme with a CC/TC cascade control was proposed to precisely maintain the product concentration for the fully heat-integrated PSD process. A comparison of the economy between atmospheric-pressurized and pressurized-atmospheric sequences indicated that the former is more energy efficient. Further, a comparison of the economy between atmospheric-pressurized and pressurized-atmospheric sequences indicated that the former is more energy efficient. This study will provide new insights into the energy efficiency and has some implications for design and control of DMC/MeOH separation in the industrialization process.

1. INTRODUCTION

A "green" chemical agent, dimethyl carbonate (DMC), is widely used because of its excellent properties,[1,2] is a building block for its superior biodegradability and low toxicity, and also an important methylating and carbonylating agent. Synthesizing DMC through the urea methanolysis method is a green route with numerous advantages: the raw materials (urea and methanol) are cheap and easy to obtain, main products are of high-quality DMC, and less impurity content (byproduct ammonia).[3−6] Especially, higher reaction activities and higher product selectivity of this reaction route make it a safe and simple process and thus, the cost of production of DMC could be significantly lowered. However, for a minimum-boiling homogenous azeotrope DMC/MeOH generated under atmospheric pressure, it is difficult to achieve effective separation using traditional distillation. Under the double pressure of the environment and resources, it is one of the effective ways to solve the energy crisis with the utilization of green separation process.

Several enhanced distillation techniques had been developed to separate azeotropic mixtures, such as azeotropic, extractive, pressure swing, and salt-addition distillation. Pressure-swing distillation (PSD), a contamination-free and environmentally friendly separation method,[7−13] which avoids the disadvantage of addition of an entrainer compared with extractive distillation, is superior to other methods due to various advantages, such as low operating costs, shortened process,

Received: February 1, 2023
Accepted: May 11, 2023
Published: June 2, 2023

easy control, simplicity of operation, and so on. This technology displays remarkable separation performance for azeotrope separation.

Recently, several schemes have been proposed in a large collection of literature studies to develop the DMC/MeOH separation strategy via PSD. Li et al.[14] proposed an atmospheric-pressured rectification process and regressed the binary interaction parameters of the UNQUAC model between MeOH and DMC. Zhang et al.[15] investigated an atmospheric-pressured separation method for separating the azeotrope produced via a urea methanolysis process, optimal parameters were also proposed. In our previous research,[16] an atmospheric-pressured process based on the Wilson coefficient model was proposed and global economic analysis was used to develop a rigorous steady-state simulation.

Huang et al.[17] developed an innovative transesterification process for synthesizing DMC, which integrated reactive distillation and PSD technologies, the results indicate that the improved process can cut 18.6% of energy loss and 99.9% conversion rate of propylene carbonate can be achieved. An et al.[18] proposed an intensified reactive PSD process that could achieve a total energy cost saving of 46.0%, a total annual cost (TAC) saving of 34.3%, and a reduction of 45.0% in CO_2 emissions, compared to the traditional heat-integrated PSD process. It is found to be an efficient and environmentally friendly technology.

In the current study, there are still weaknesses in PSD technologies, most notably a high energy consumption and low thermodynamic efficiency. A growing number of scholars have been interested in improving the thermodynamic efficiency of PSD process, and numerous studies have now found that remarkable energy savings can be achieved through the PSD process with heat integration.[19−33] These findings indicate that the heat integration process has a higher thermal efficiency, less energy consumption, greater economic advantages, and environmental benefits than the conventional ones. However, this energy-saving and efficient technology makes the process complex and difficult to control. Thus, effective control of heat-integrated PSD process has become a key bottleneck preventing its further improvement. Recently, many scholars have conducted a considerable amount of research on control of heat-integrated PSD process. Luyben[34] investigated the dynamic performance of the fully and the partially heat-integrated systems for THF/water separation, and the results showed that only small disturbance can be accommodated. Yu[35] presented several fully heat-integrated control systems for methyl/MeOH separation and proposed a pressure-compensated temperature control (PCTC), which works fairly well for the fully heat-integrated process in terms of large feed disturbances. Zhu et al.[24] explored three PSD schemes for separating acetonitrile/methanol/benzene with no, partial, and full heat integration, the fully heat-integrated process was found to be more efficient and economical than others, but its dynamic performance is inferior to that without heat integration. Shan et al.[36] developed three partial and one full integration processes for THF/ethanol/water separation and compared their control and economy, the results showed that the controllability of the full integration process was slightly inferior to the ones without heat integration. These studies[37,38] could accelerate the advance in the control strategy of heat-integrated PSD processes and broaden the applications of process design and control in industries.

In recent years, a little attention was paid to improving the thermodynamic efficiency and dynamic controllability of PSD systems for DMC/MeOH separation. In previous studies, we proposed a pressured-atmospheric distillation process for DMC/MeOH azeotrope separation and a dual-temperature control strategy to effectively handle 20% feed disturbances. However, there were few recommendations in this study in terms of the design and control strategy for the energy-saving process. Zhang et al.[39] proposed a pressured-atmospheric distillation system via partial heat integration for DMC/MeOH azeotrope separation, which could reduce 20.01% TAC than the one without heat integration, and a composition/temperature cascade control structure exhibited robust dynamic performance when 20% feed disturbances are introduced. However, most of this work has studied the design and control of the process with partial heat integration, the controllability and economy of the process with and without heat integration was not systematically discussed.

In this article, the economy and controllability of the DMC/MeOH separation process with no, partial, and full heat integration were systematically explored. Initially, an atmospheric-pressurized process was presented, rigorous steady-state optimization of the atmospheric-pressurized process with and without heat integration were carried out via sequential iteration optimization algorithm. Further, the controllability of the with and without heat-integrated processes were investigated in detail. A PCTC scheme with a CC/TC cascade control was proposed to precisely maintain the product concentration for the fully heat-integrated PSD process. Finally, the two sequences of atmospheric-pressurized process and pressurized-atmospheric[15] process was compared in terms of economy. This study will provide some implications for design and control of DMC/MeOH separation in the industrialization process.

2. STEADY-STATE DESIGN

2.1. DMC−MeOH System. Process data for atmospheric-pressured conditions are as follows: 10.963 kmol/h fresh

Table 1. Binary Interaction Parameters of the Equations[a]

parameter	b_{ij}	b_{ji}	c_{ij}
Wilson	−333.61	−159.07	0

[a]Where i and j represent the DMC and MeOH, respectively.

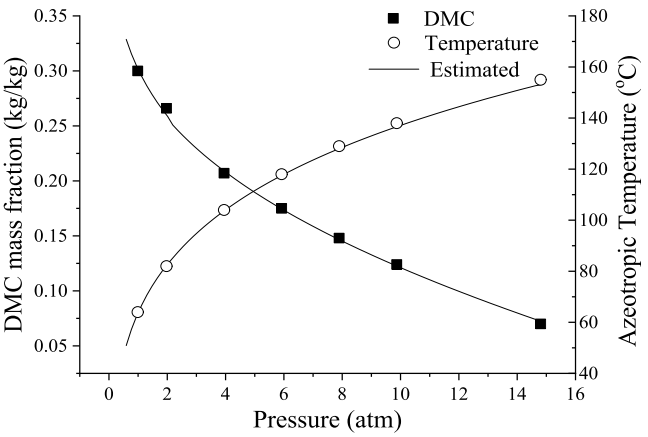

Figure 1. Experimental data of DMC and MeOH mixtures at different pressures and its prediction with the Wilson model.

https://doi.org/10.1021/acsomega.3c00656
ACS Omega 2023, 8, 20450−20470

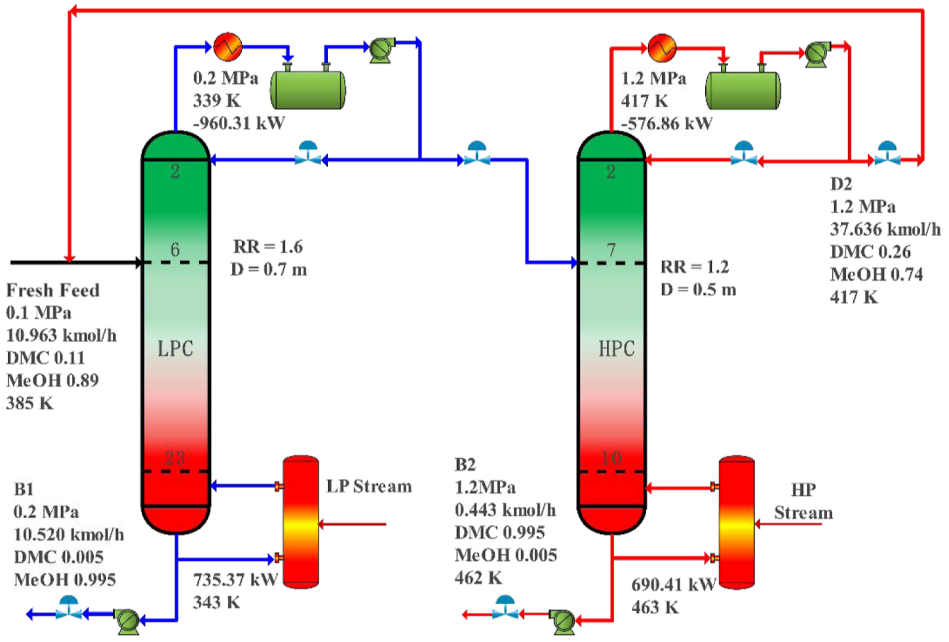

Figure 2. LP-HP flowsheet with the feed conditions, heat duty, and reflux ratio.

Table 2. Design Variables and TAC of the System with Heat Integration

	no heat integration		partial heat integration		full heat integration	
	LP	HP	LP	HP	LP	HP
Nstage	24	11	24	11	24	11
feed stage	6	7	6	7	6	7
D (m)	0.7	0.5	0.7	0.5	0.7	0.6
Q_R, (kW)	735.3684	690.4104	−918.7280		−880.25	
Q_C, (kW)	−960.3080	−576.8637	82.3626	724.9670		768.86
A_C, (m^2)	10.0455	6.0344	9.6106		9.2081	
A_R, (m^2)	14.8034	13.8984	1.6580	14.5940		15.4776
shell, ($10^6$$)	0.1076	0.0364	0.1050	0.0374	0.1026	0.0387
HX, ($10^6$$)	0.0747	0.0638	0.0419	0.0417	0.0301	0.0433
energy, ($10^6$$/y)	0.1090	0.1023	0.0122	0.1075		0.1140
capital, ($10^6$$)	0.1842	0.1003	0.1469	0.0791	0.1335	0.0820
TAC, ($10^6$$/y)	0.1698	0.1385	0.0612	0.1338	0.0445	0.1413
total capital ($10^6$$)	0.2827		0.2260		0.2155	
total energy ($10^6$$/y)	0.2113		0.1197		0.1140	
TAC ($10^6$$/y)	0.3056		0.1950		0.1858	

flowrate with 89.1 wt % MeOH and 10.9 wt % DMC and a small amount of NH_3 and CO_2. The Wilson physical property package in Aspen Plus is used to perform rigorous steady-state simulations. The Wilson equation is given below

$$\gamma_i = 1 - \ln\left(\sum_j \tau_{ij}x_j\right) - \sum_j \frac{\tau_{ji}x_j}{\sum_k \tau_{jk}x_k} \quad (1)$$

whereln $\tau_{ij} = a_{ij} + \frac{b_{ij}}{T} + c_{ij}\ln T + d_{ij}T$

The estimated regression parameters are shown in Table1:

The mixture of DMC/MeOH forms a minimum binary azeotropic mixture at 64 °C with 70 MeOH:30 DMC wt % under atmospheric pressure. As shown in Figure 1, the experimental data of DMC and MeOH mixtures at different pressures and its prediction with the Wilson model is compared, and the consistency between the measured values and calculated values is good. The DMC concentration gradually decreases as pressure increases. It is quite clear that a PSD process should be feasible and the pressure of the pressured column is selected to be 1.2 MPa. The desired product concentration in this binary system is assumed to be 99.5 wt % DMC and 99.5 wt % MeOH at the bottom of LP and HP columns, respectively. Useful information for using these simulators is obtained from Luyben.[40]

2.2. No Heat Integration in the Steady-State Simulation. Flowsheet for atmospheric(LP)-pressurized(HP) flowsheets with no heat integration is shown in Figure 2. The fresh feed is sent to T1 at near 0.2 MPa, high purity MeOH (≥99.5 wt %) is then run off from the bottom of T1, and a composition close to a new azeotrope(74 wt % MeOH and 26 wt % DMC) is distilled from the top. The overhead product then flows into T2 (operated at 1.2 MPa), a high-concentration DMC runs off from the bottom of T2, and the overhead distillate is recycled back to T1.

The "Design Spec/Vary" function in Aspen Plus is used to achieve the product concentration required in each column.

https://doi.org/10.1021/acsomega.3c00656
ACS Omega 2023, 8, 20450−20470

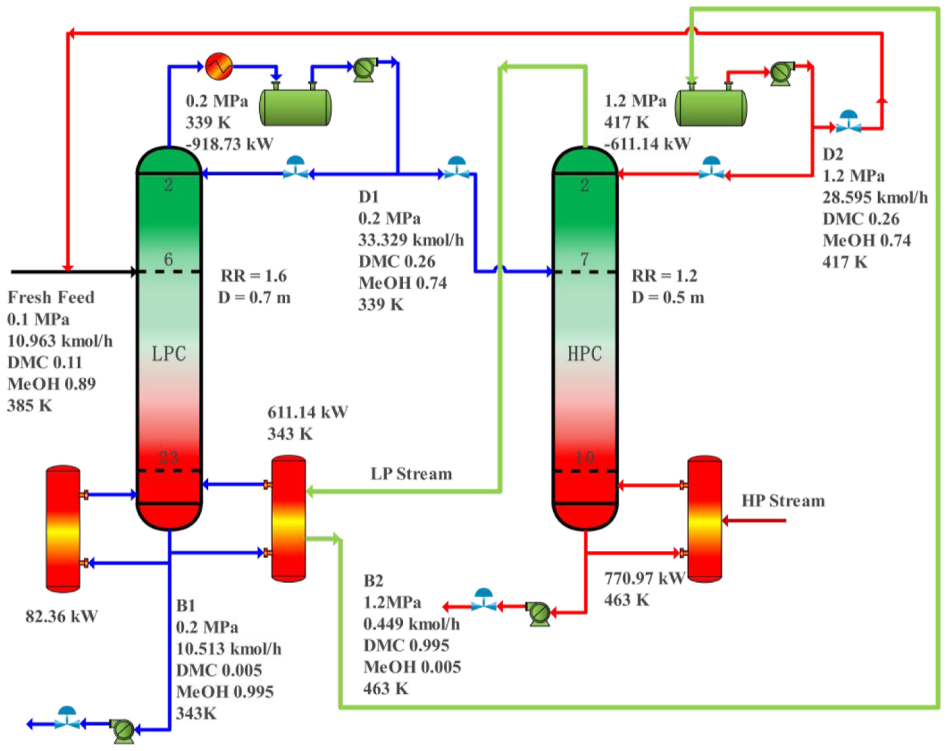

Figure 3. LP-HP distillation flowsheet with partial heat integration.

Several design degrees of freedom exist in this LP-HP distillation system: the number of trays (N_T), the feed tray location (N_F), the distillate flowrate D, and the reflux ratio RR. By minimizing the TAC of the whole system, the optimal operating conditions were determined. Traditionally, TAC has been adopted as the objective function to be minimized by adjusting parameters (N_T, N_F, etc.) in the design. "Tray sizing" function in Aspen Plus was used to determine the size of the two columns, and sieve plate was selected. Condenser and reboiler heat-transfer areas are calculated by the overall heat-transfer coefficient and condenser/reboiler temperature difference. After optimization of the parameters, the optimal design variables and the minimum TAC of the LP-HP distillation system with no heat integration are shown in Table 2.

The flowsheet with detailed simulation results is shown in Figure 2. The reboiler heat input is 735.37 kW for the LP column and 690.41 kW for the HP column, respectively. The condenser heat removal is 960.31 kW for the LP column and 576.86 kW for the HP column, respectively. Notably, the reflux drum temperature of the HP column (417 K at 1.2 MPa) is higher than the bottom temperature of the LP column (339 K at 0.2 MPa); thus, heat integration should be considered to decrease the energy consumption.

2.3. Partial Heat Integration in the Steady-State Simulation. Achieving partial heat integration in this system requires that Q_{C2} not be completely equal to Q_{R1}, that is, an auxiliary reboiler is required. As shown in Figure 3, Q_{C2} is used as a portion of Q_{R1}, with a steam-heated auxiliary reboiler heated by the LP stream providing the remaining heat. The reboiler in the HP column was driven by the HP stream.

Partial heat integration optimization using the sum of the LP column auxiliary reboiler duty Q_{aux} and the HP column reboiler duty Q_{R2} as the total energy consumption. Based on the no integration optimization results, optimization procedures for partial heat integration are as follows:

By manipulating the flowrates of the two streams at the bottom, two product purities are maintained by the Aspen "Design Spec/Vary" function. In both columns, reflux ratios are the variables for design optimization, which are varied until the reboiler energy consumption (the sum of Q_{R1} and Q_{R2}) is minimized. The optimization results are RR_1 = 1.6 and RR_2 = 1.2.

The optimized operating parameters of the partial heat integration system are shown in Figure 2, and the total energy consumption is 807.33 kW (Q_{R1} = 82.36 and 724.97 kW). In this case, the HP column condenser's heat load is −611.14 kW. The partially heat-integrated process could be recommended here for energy saving, which has been widely investigated in the open literature.

A condenser could transfer 918.73 kW of energy into the column and a stream-heated auxiliary reboiler could supply the remaining energy requirement of 693.50−611.14 = 82.36 kW. The heat-transfer coefficient is chosen to be 3.06 × 10^{-3} GJ h^{-1} m^{-2} °C (0.85 kW/(K·m^2)), and the area of the auxiliary reboiler is 1.6580 m^2.

The optimal system parameters and various cost data of this system with partial heat integration are revealed in Table 2. Figure 3 demonstrates the partially heat-integrated process with detailed stream information, operating conditions, equipment sizes, and heat duties under steady-state conditions.

2.4. Full Heat Integration in the Steady-State Simulation. In this part, the LP-HP flowsheet with full heat integration is studied. The heat input Q_{R2} in the HP column is the only energy input. The "Design spec/Vary" feature in Aspen Plus is used to adjust the bottom flowrates to achieve the product concentration (99.5 wt % MeOH in the LP column and 99.5 wt % DMC in the HP column).

To achieve full heat integration, the sum of the condenser heat removal Q_{C2} in the HP column (a negative value here) and the reboiler heat input Q_{R1} in the LP column must equal 0;

https://doi.org/10.1021/acsomega.3c00656
ACS Omega 2023, 8, 20450−20470

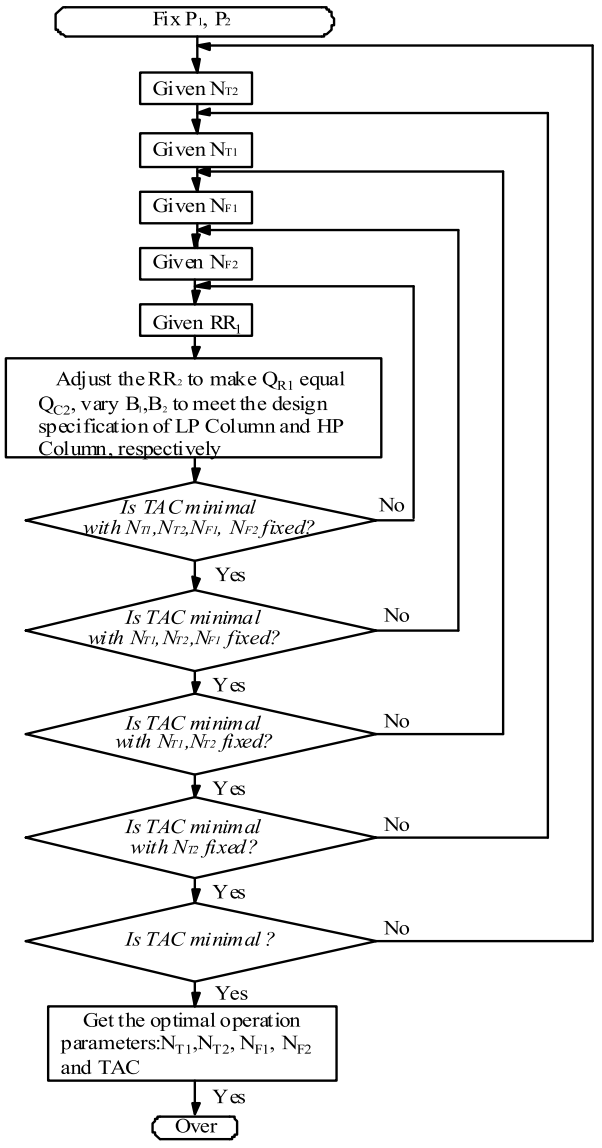

Figure 4. Optimal sequence for the fully heat-integrated PSD process.

that is, it reaches a minimum for total energy consumption though this "neat" configuration. Meanwhile, the requirement that the reboiler heat input Q_{R1} be equal to the condenser heat removal rate Q_{C2} results in a loss of degrees of freedom. Figure 4 illustrates a sequential iterative optimization sequence for the fully heat-integrated PSD process.

In addition, the full optimization is guided by the following optimization procedures: (1) in Aspen Plus, the "Design Spec/Vary" features was used to adjust the bottom flowrate in each column block to meet the desired purity level. It is the same specification for the product purities in all cases. (2) In order to run steady-state simulations in Aspen Plus that rigorously capture the neat heat integration, the "flowsheet design specification" was used to make "$Q_{R1} = -Q_{C2}$". RR_2 in the HP column was chosen as the manipulated variable. Thus, RR_2 was varied by the flowsheet design spec to make "$Q_{R1} = -Q_{C2}$". (3) Fixing the reflux ratio RR_1 in the LP column, three variables (B_1, B_2, and RR_2) were used to achieve the two product compositions and to make the magnitude of the heat duties equal while the sign is opposite. (4) Next, varied RR_1 to minimize the heat input to the reboiler of the HP column Q_{R2}.

The reflux ratio in the HP column RR_2 was selected to be the manipulated variable, which was varied in the "flowsheet design spec" to make Q_{R1} equal to $-Q_{C2}$. As shown in Figure 5, the optimum reflux ratio RR_1 is 1.5, the corresponding total heat input Q_{R2} is 139.61 kW, Q_{C2} is −612.3 kW, and RR_2 is 1.30.

The detailed simulation results of the fully integrated system are illustrated in Table 3 and the design conditions and cost data for the LP-HP distillation system with full heat integration are illustrated in Table 2; overall estimates of equipment sizing and capital costs are borrowed from Luyben and Turton.[41] The economizers are sized with the selection of a minimum range of temperatures from 10 to 15 °C. The total heat-transfer coefficient is chosen to be 3.06×10^{-3} GJ h^{-1} m^{-2} °C (0.85 kWm^{-2} °C). The temperature difference in the condenser of the LP/HP column and a suitable total heat-transfer coefficient can be used to calculate the heat-transfer area; the calculated heat-transfer area of the heat exchanger is 10.45 m^2.

The steady-state flowsheet with full heat integration is illustrated in Figure 6, which includes details of the operating

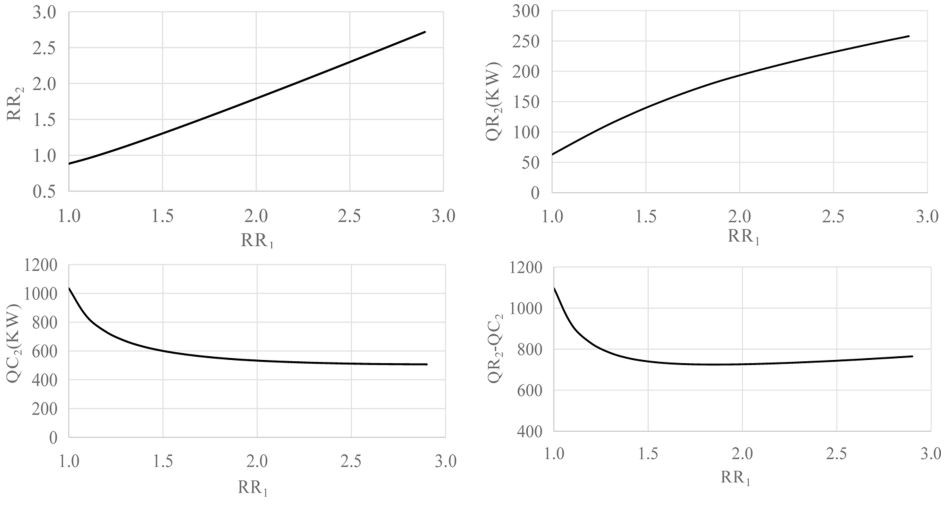

Figure 5. Effect of RR_1 on Q_{R2}, Q_{C2}, and RR_2.

https://doi.org/10.1021/acsomega.3c00656
ACS Omega 2023, 8, 20450−20470

Table 3. Simulation Results of the Process with Full Heat Integration

	F	D_2	B_2	D_1	B_1
temperature, (K)	385.1	341.4	453.7	339.1	343.3
pressure, (MPa)	0.493	0.118	0.91	0.109	0.124
mole flow, (kmol/h)	10.963	32.877	0.449	33.326	10.512
mass flow, (kg/s)	0.105	0.343	0.011	0.351	10.094
enthalpy, (MMBtu/h)	−2.204	−7.984	−0.243	−8.569	−2.335
density, (lb/cuft)	0.336	0.327	14.420	49.918	46.348
mass flow, (kg/s)					
DMC	0.012	0.074	0.011	0.085	0.001
MeOH	0.093	0.266	5.56×10^{-5}	0.266	0.093
mass frac					
DMC	0.11	0.217	0.995	0.242	0.005
MeOH	0.89	0.783	0.005	0.758	0.995

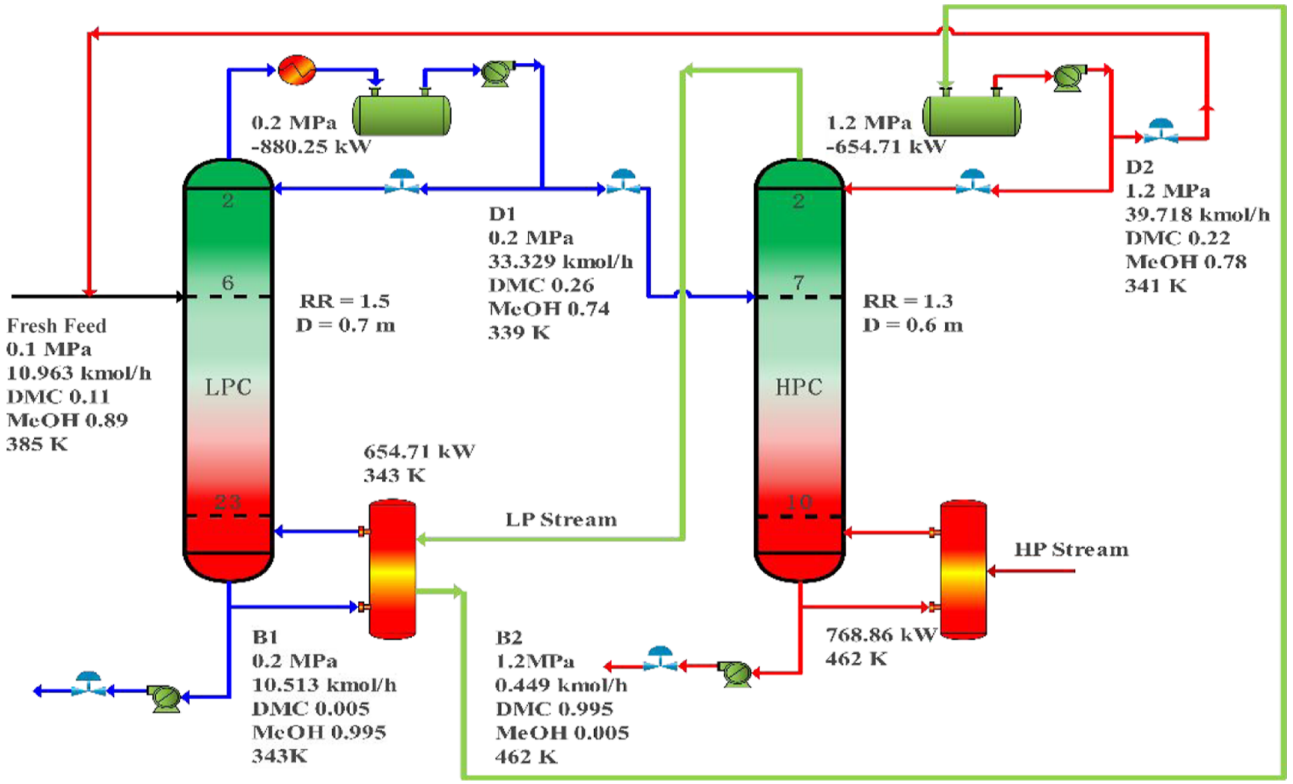

Figure 6. LP-HP distillation flowsheet with full heat integration.

conditions, stream information, thermal load, and equipment sizing.

Using TAC as the objective function, a detailed comparison economic is obtained (Table 2). The TAC of the overall process with full heat integration is $0.1858*10^6$\$/y, the TAC with no heat integration is $0.3056*10^6$\$/y, and the TAC of the overall process with partial heat integration is $0.1950*10^6$\$/y. These results show that separation via full heat integration can cut the TAC by as much as 39.2% and that partial heat integration can reduce the TAC by as much as 36.2%.

The behaviors of the temperature and concentration profiles for the LP-HP system are demonstrated in Figure 7. A sharp composition change is observed near the ninth tray of the HP column as DMC gathers at the bottom of the HP column and MeOH gathers at the bottom of the LP column. A fairly steep temperature slope is also observed near the ninth tray of the HP column. Therefore, the ninth tray is chosen as a sensitive plate for the HP column, and the twentieth tray is chosen as a sensitive plate for the LP column.

3. CONTROL SYSTEM DESIGN

After the reflux drum and base volume were specified, Aspen Plus files were converted into pressure-driven dynamic simulations, when the vessels were half full, the flash drum was sized to provide 5 min of holdup. The majority of valves were specified to have pressure drops of approximately 300 kPa, and pumps were inserted to provide adequate pressure drops over valves. The default control strategy[42−45] is reconstructed as discussed below.

3.1. System with No Heat Integration. When the process is not heat-integrated, the two columns have independent condensers and reboilers. The bottom temperature and the reflux ratio in each column can be used as simultaneously controlled variables. Accordingly, the bottom temperature changes immediately with the heat input to the

https://doi.org/10.1021/acsomega.3c00656
ACS Omega 2023, 8, 20450−20470

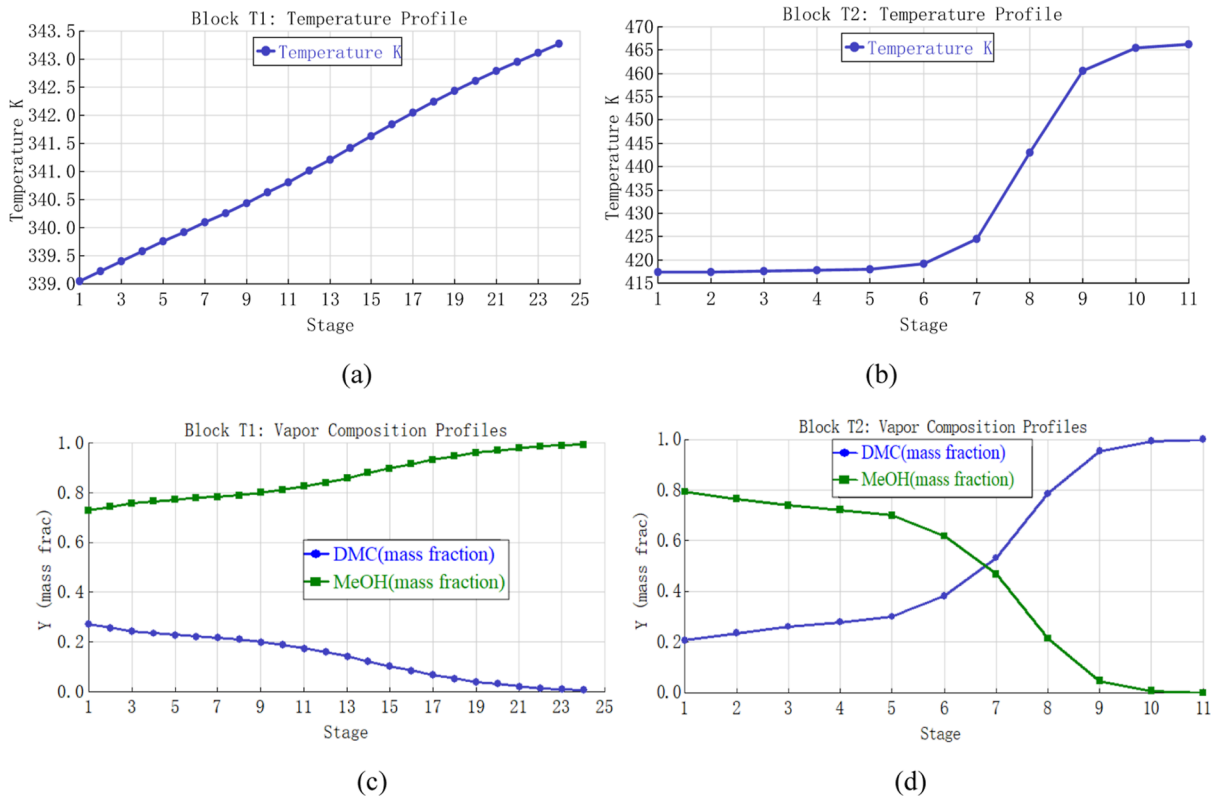

Figure 7. (a) LP column: temperature profile; (b) HP column: temperature profile; (c) LP column: composition profile; and (d) HP column: composition profile.

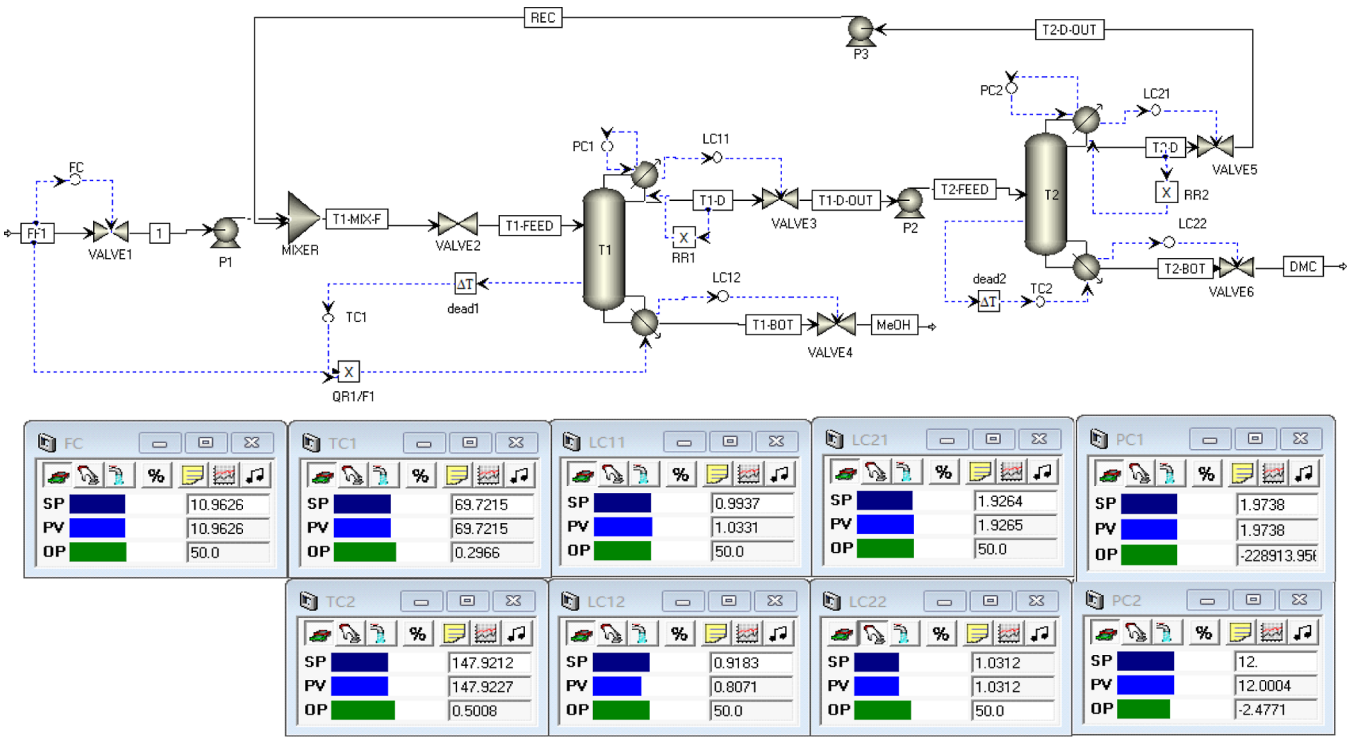

Figure 8. Nonheat-integrated control structure.

reboiler. In addition, both the two top pressures can be controlled.

Except for four liquid level controllers, all other controllers used PI controllers. Level controllers on both columns were proportional with a gain of 2. Pressure loops on both columns had proportional and integral settings of Kc = 20 and τ_1 = 12 min. The proportional and integral settings on the flow control loops for both columns were Kc = 0.5 and τ_1 = 0.3 min. 1 min

https://doi.org/10.1021/acsomega.3c00656
ACS Omega 2023, 8, 20450−20470

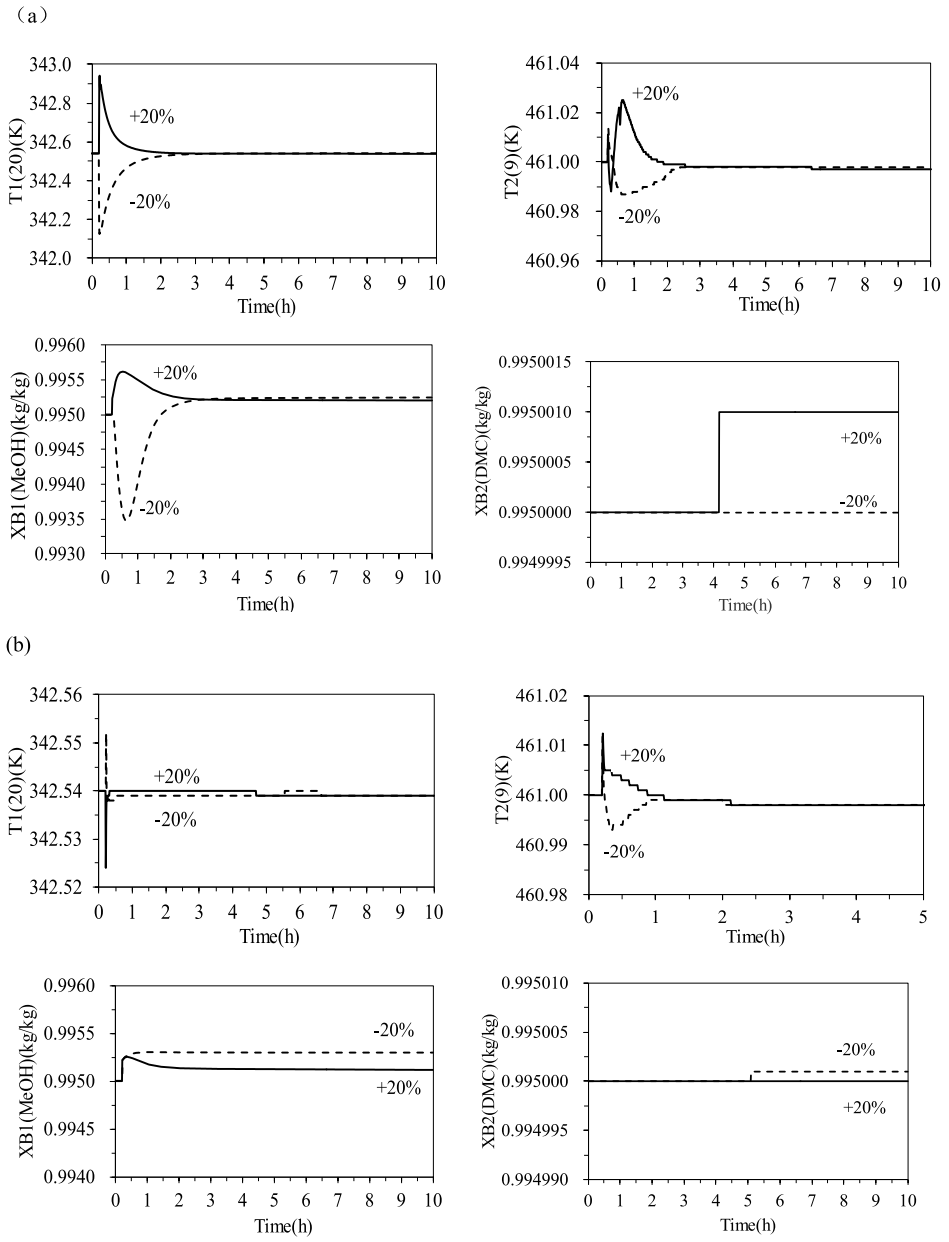

Figure 9. Dynamic responses for the nonheat-integrated process: (a) feed flowrate disturbances. (b) Feed composition disturbances.

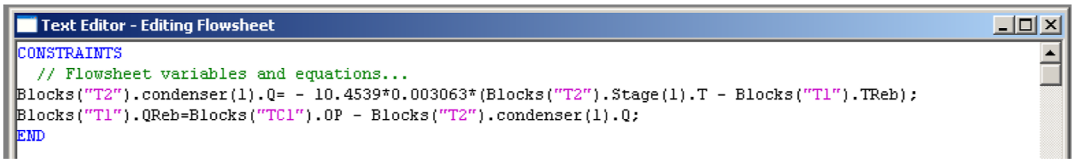

Figure 10. Flowsheet equation with an auxiliary reboiler.

was set as the deadtime for the temperature controller. Based on Tyreus and Luyben tuning rules provided in Aspen Dynamic, tuning constants were determined via relay feedback tests. LP column temperature loops were tuned first by the iterative tuning procedure and then HP column temperature loops. In this procedure, the tuning parameters from the relay feedback test were repeated until convergence is achieved.

Figure 8 illustrates this control scheme, in which two reboiler heat inputs are manipulated by two-temperature controllers, respectively. The pressure in the HP column is controlled, and the reflux ratio in each column remains fixed. A Q_{R1}/F ratio controller, with its ratio reset by TC1, is used in the LP column.

The characteristics of the loops are as follows:

(1) The pressure in each column is controlled by manipulating the condenser heat removal (reverse acting).

(2) The reflux ratio in each column is controlled.

(3) The feed is flow-controlled (reverse acting).

https://doi.org/10.1021/acsomega.3c00656
ACS Omega 2023, 8, 20450−20470

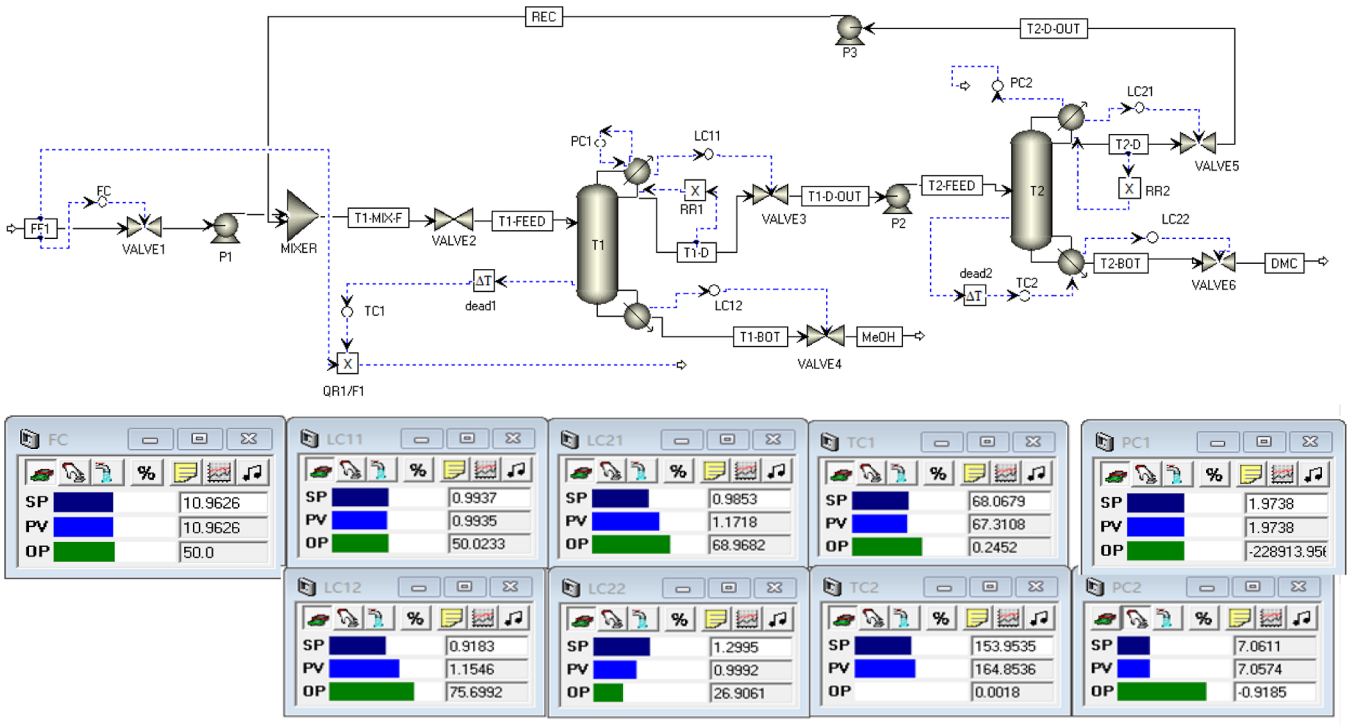

Figure 11. Control structure with the partial heat integration-PHICS1.

(4) The reflux drum level in each column is controlled by manipulating the distillate flow (direct acting).
(5) The temperature on stage 20 in the LP column is controlled by manipulating the reboiler heat-input-to-feed ratio (Q_{R1}/F_1).
(6) The base level of each column is controlled by manipulating the bottom flowrate (direct acting).

Dynamic performance of the control scheme NHICS was evaluated with 20% flowrate and composition disturbance tests. Figure 9a,b demonstrates the performance of the NHICS for a 20% step change in the feed flowrate and composition disturbances, respectively. Solid lines depict a 20% step increase while dashed lines represent a 20% step decrease at 0.2 h.

As shown in Figure 9, the product purities X_{B1}(DMC) and X_{B2}(MeOH) are very close to their set point of 99.5 wt % during the transient disturbances. The transient deviation in X_{B1}(MeOH) is approximately 2200 ppm, and the transient deviation in X_{B2}(DMC) is below 1 ppm for large disturbances in the feed flowrate. Figure 9a demonstrates the dynamic performance of this system for a 20% increase and decrease in feed composition disturbances at 0.2 h. The transient deviation in X_{B1}(MeOH) is approximately 175 ppm and the transient deviation in X_{B2}(DMC) is approximately 1 ppm for these composition disturbances.

Altogether, the transient deviations in both X_{B1}(MeOH) and X_{B2}(DMC) are very small in the face of 20% feed disturbances. These results indicate that the nonheat-integrated system exhibits good dynamic performance.

3.2. System with Partial Heat Integration. *3.2.1. Basic Control Structure PHICS1.* The "Flowsheet Equations" function in Aspen Dynamics was used to implement the partial integration control (Figure 10). HP column heat removal rate Q_{C2} and the input to the auxiliary reboiler Q_{aux} were calculated from the first and second equations, respectively. For partial heat integration, no pressure controller was used on the HP column, it floated depending on operating conditions. Furthermore, in the LP column, the reboiler heat input was not specified. As shown in Figure 11, the temperature controller loop in the LP column was disconnected from the pressure controller in the HP column and the top pressure indicator in the HP column was set to manual.

After compiling the flowsheet equations, two variables—the reboiler heat load to the LP column Q_{R1} and the condenser load in the HP column Q_{C2}—were overspecified, which must be changed from "fixed" to "free". These changes were achieved by implementing the following operations: clicked on the respective column, selected "forms" and "all variables" and scrolled down to the appropriate variable; changed the variables "Q_{Reb}" (LP column) and "condenser(1). Q_R" (HP column) from "fixed" to "free", respectively. The partial heat integration flowsheet is now correctly specified.

Figure 11 displays the basic control strategy of the system with partial heat integration. A feed forward ratio control structure "Q_{aux}/F_1" is added between the feed and the heat input to the auxiliary reboiler to improve dynamic performance. The output signal from temperature controller TC1 is one input to the feedforward controller "Q_{aux}/F_1", and the output of the multiplier "Q_{aux}/F_1" is disconnected. The auxiliary reboiler heat input "Q_{aux}" is proportional to the feed rate F_1, and the ratio is adjusted by TC1. A multiplier block is used to set up this ratio scheme, with the feed flowrate F (kmol/h) and the ratio "Q_{R1} (GJ/h) to F" as two input variables. According to our simulation results, the auxiliary reboiler duty is 76.66 kW (0.28 GJ/h) and Q_{aux}/F_1 = (0.28 GJ/h)/(10.96 kmol/h) = 0.0255.

As shown in Figure 12a, the response of PHICS1 with 20% step changes in the feed flowrate illustrates that stable regulatory control can be achieved.

https://doi.org/10.1021/acsomega.3c00656
ACS Omega 2023, 8, 20450−20470

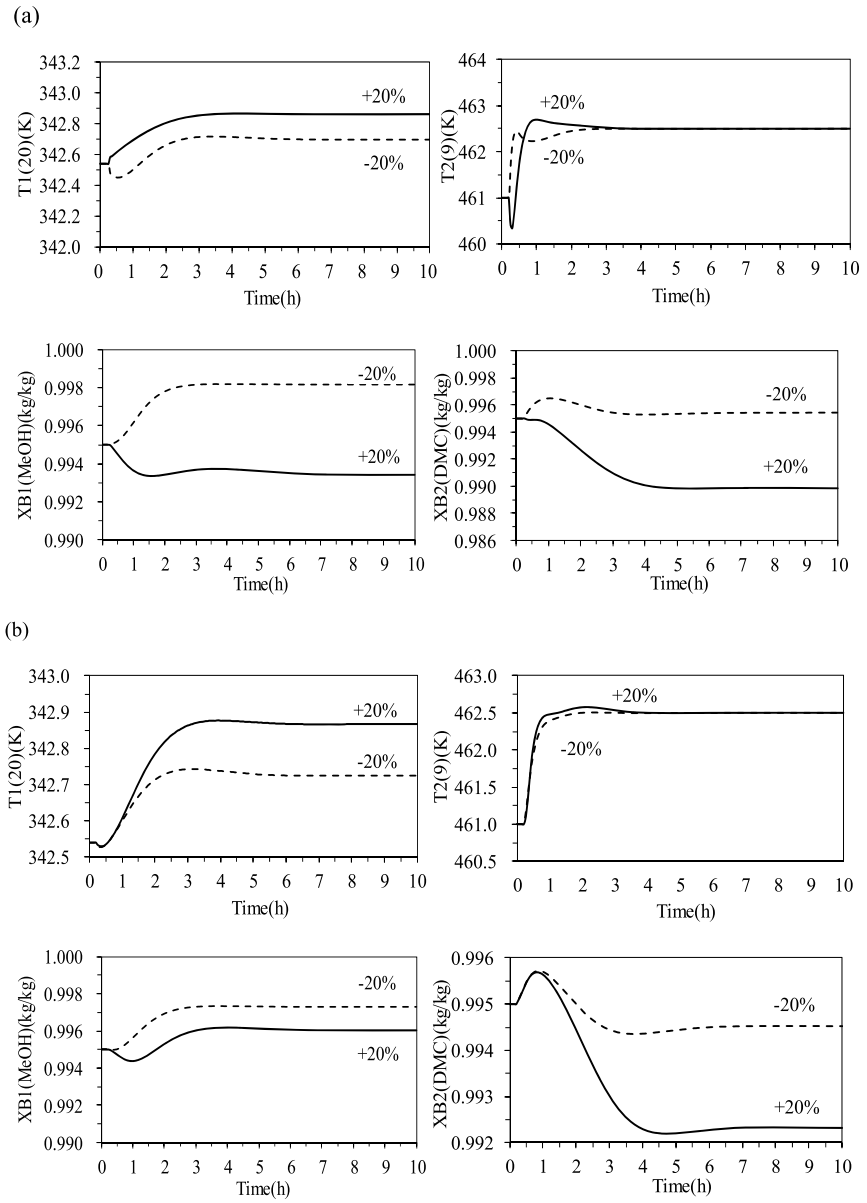

Figure 12. Dynamic responses for PHICS1: (a) 20% feed flowrate disturbances and (b) 20% feed composition disturbances.

Similar results are observed in Figure 12b for a 20% increase and decrease in the feed composition at 0.2 h. The largest transient deviation of X_{B2}(DMC) decreased from 0.995 to 0.990 wt % for the +20% feed flowrate disturbance, and the largest transient deviation of X_{B2}(DMC) decreased from 0.995 to 0.992 wt % for the +20% feed composition disturbance.

The largest transient deviation of X_{B1}(MeOH) decreased from 0.995 to 0.993 wt % for the +20% feed flowrate disturbance, and the transient deviation in X_{B1}(MeOH) is very small for feed composition disturbances, whereas a slight deviation in X_{B2}(DMC) is observed in other cases.

It was observed that regardless of a +20% flowrate and composition disturbance, the system handles these disturbances well, except for the bottom purity X_{B2} (DMC). While the transient deviation of X_{B2}(DMC) was more significant than that of X_{B1}(MeOH). Particularly, it took more time for X_{B2}(DMC) than X_{B1}(MeOH) to regain stability after deviation.

3.2.2. Improved Control Structure PHICS2. A ratio block, where the reboiler heat load Q_{R1} of the LP column is proportional to feed flowrate F, is used to improve the dynamic performance of PHICS1. This improved structure with an additive feed forward scheme is shown in Figure 13.

The total reboiler heat duty of the LP column is then given as the output signal of the multiplier block "Q_{Rtot}/F", which acts as one input signal of a summation block; another input signal of the summation block is from "TC1" but opposite in sign, and the output signal of the summation block is the heat-transfer rate of the auxiliary reboiler Q_{aux}. With such a structure, the steam flow to the reboiler will immediately change as the feed flowrate changes. Here, the auxiliary reboiler Q_{aux} is adjusted by the temperature controller "TC1" to trim up the heat input. The total heat input Q_{R1} is the sum of Q_{aux} and Q_{C2} (negative in sign), and the ratio of "Q_{Rtot} to F" is (2.64 GJ/h)/(10.963 kmol/h) = 0.24. Additionally, the ratio could be adjusted via the HP column temperature controller

https://doi.org/10.1021/acsomega.3c00656
ACS Omega 2023, 8, 20450−20470

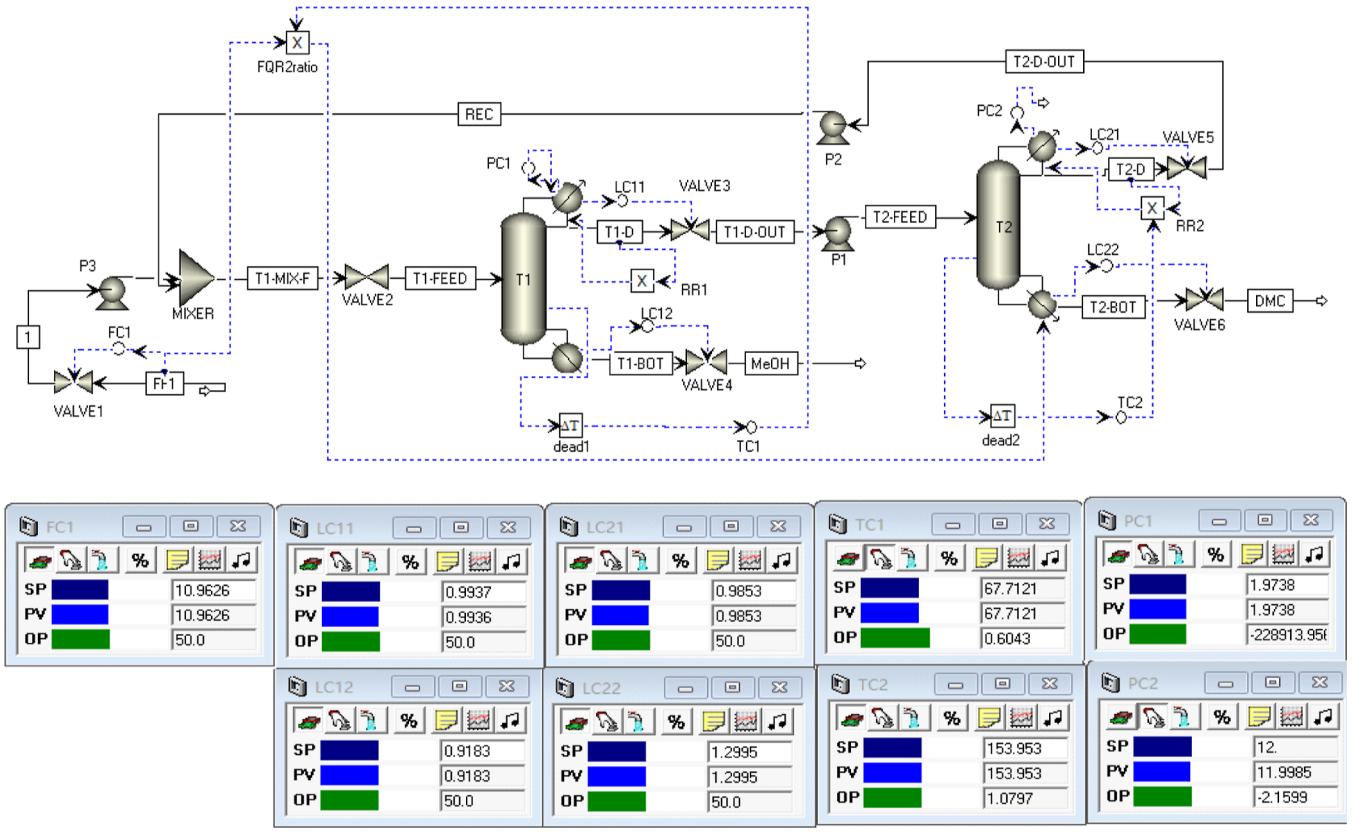

Figure 13. Control structure with an auxiliary reboiler and ratio-PHICS2.

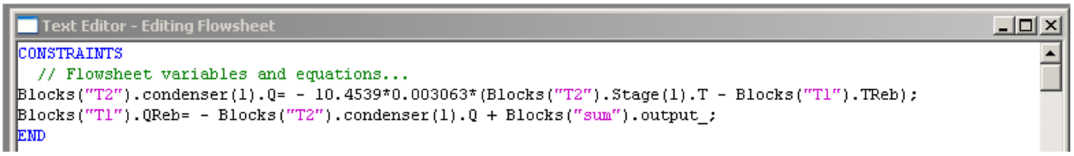

Figure 14. Flowsheet equation with the ratio.

TC2. The "flowsheet equations" function in Aspen dynamics was used to implement this control, as illustrated in Figure 14.

Using relay-feedback tests and Tyreus−Luyben tuning,[46] the ultimate gain and periods were determined. In this improved control structure, PHICS2, the tuning parameters of the two temperature controllers were changed only slightly.

The effectiveness of the partial heat integration system for a 20% step in the feed flowrate and feed composition is demonstrated in Figure 15a,b, respectively. The largest transient deviation of X_{B2}(DMC) decreased from 0.995 to 0.991 wt % for the +20% feed flowrate disturbance, and the largest transient deviation of X_{B2}(DMC) decreased from 0.995 to 0.993 wt % for the +20% feed composition disturbance. These changes occur because the changes in the parameters for the HP column are not floating under the operating conditions. The Q_{R1} and Q_{R2} increase with increasing feed flowrate. Figure 15a,b also reveals that the improved control structure PHICS2 performed well for these large disturbances, resulting in control performances similar to those of nonheat integration.

Notably, PHICS2 usually performed better than PHICS1 for it exhibited tighter control and smaller transient deviation, while large deviations in X_{B2}(DMC) were also observed regardless of feed flowrate or composition disturbances, displaying control performances similar to those of PHICS1. This is indeed a limitation for PHICS2.

3.3. System with Full Heat Integration. Full heat integration was implemented via appropriate equations described in the text editor window (Figure 16) in Aspen Dynamics, which was achieved using flowsheet equations. The first equation calculates heat removal rate Q_{R1} of the LP column, which obeys the first law of thermodynamics. In the second equation, heat removal rate Q_{R1} and heat input rate Q_{C2} are equal but of the opposite sign. These two conditions must be satisfied simultaneously. Because the reboiler heat input Q_{R1} and condenser heat output Q_{C2} lose their degrees of freedom. These variables must, therefore, be changed from "fixed" to "free". This operation is similar to that of the partial heat integration.

For the "neat" heat integration, the LP and HP columns are highly intercoupled and interacted. Meanwhile, the heat transfer in the condenser/reboiler must be equal to the product of the area, the overall heat-transfer coefficient, and the current temperature difference between the reflux drum of the HP column and the base of the LP column.

The temperatures of the condenser/reboiler both change dynamically with pressure and composition change. The pressure in the HP column is not controlled but varies with

https://doi.org/10.1021/acsomega.3c00656
ACS Omega 2023, 8, 20450−20470

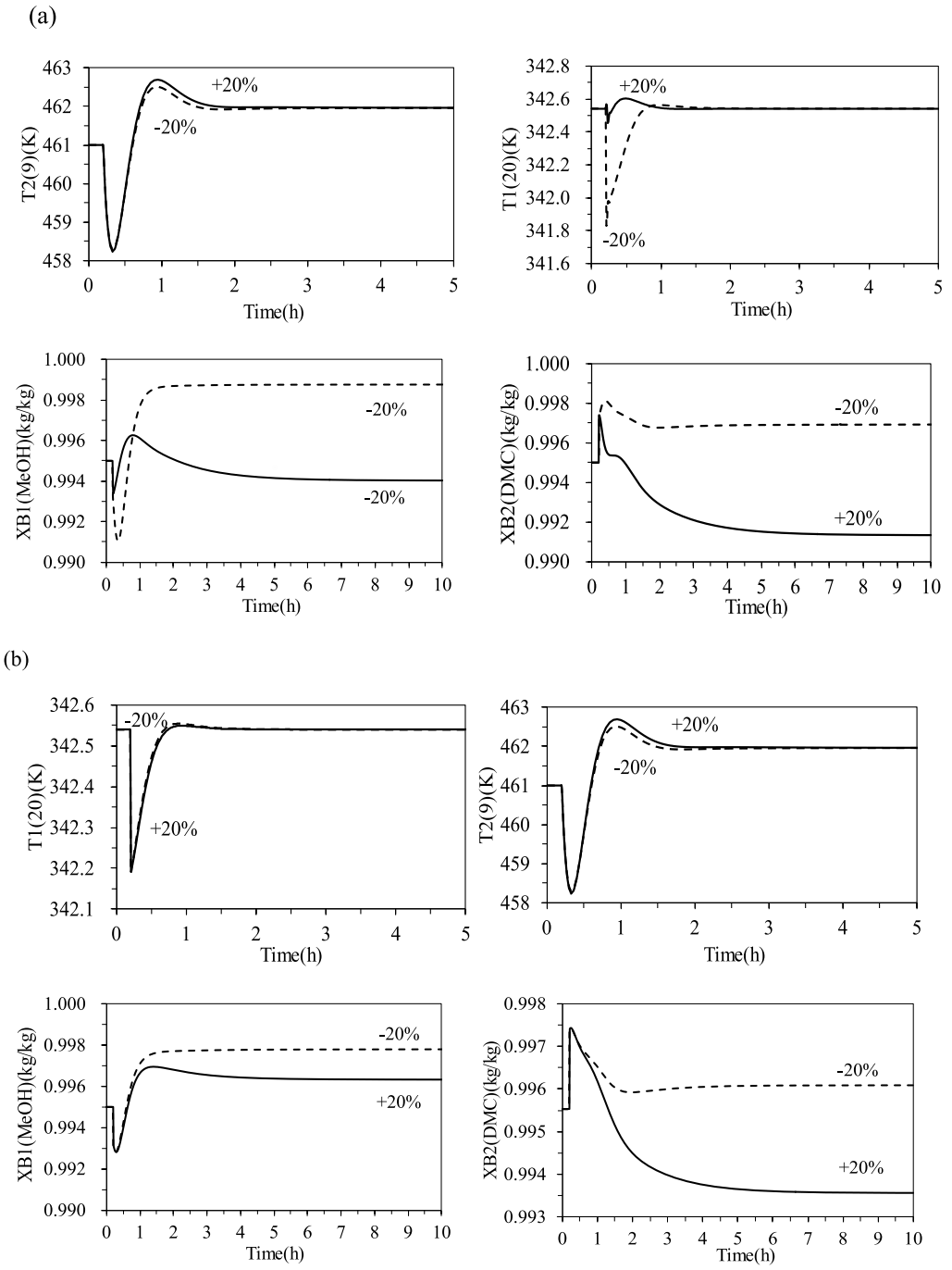

Figure 15. Dynamic responses for PHICS2: (a) 20% feed flowrate disturbances and (b) 20% feed composition disturbances.

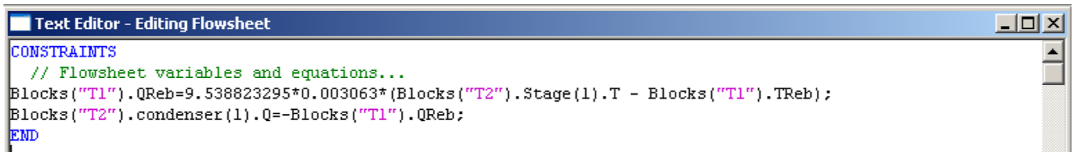

Figure 16. Flowsheet equations for condenser/reboiler coupling and heat transfer.

operating conditions. A disturbance in the LP column can be directly transmitted to the HP column, which will inevitably lead to control issues.

3.3.1. First Control Structure FHICS1. The preliminary control structure—FHICS1, in which two reflux ratios RR_1 and RR_2 are both fixed, is shown in Figure 17. With the exception of the default controller, three features differ from those of the other control structures: the pressure P2 in the HP column is not controlled but floats (on manual); the output signal of TC1 is Q_{R2}, and the output signal of TC2 is RR_2. The temperature controller TC2 is "direct acting". This control system operates steadily. Making the reflux ratio fixed in the

https://doi.org/10.1021/acsomega.3c00656
ACS Omega 2023, 8, 20450−20470

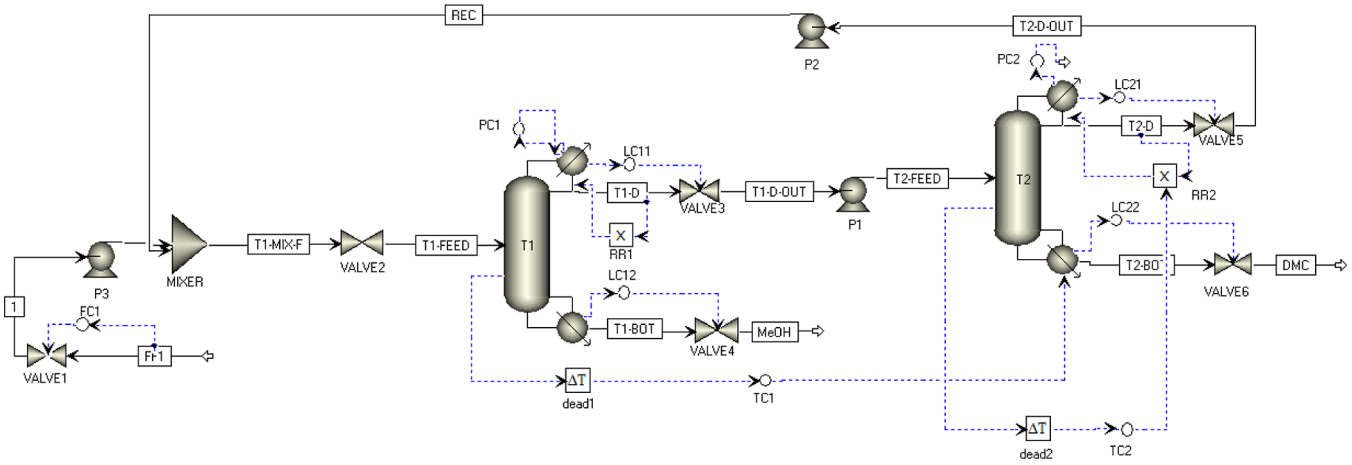

Figure 17. Preliminary control structure-FHICS1.

Table 4. Temperature Controller Tuning Parameters for Each Control Structure

parameters	NHICS	PHICS1	PHICS2	FHICS1	FHICS2	PCTC
	TC1	TC1	TC1	TC1	TC1	TC1
controlled variable	$T_{1,20}$ = 340	$T_{1,20}$ = 341	$T_{1,20}$ = 341	$T_{1,20}$ = 340.7	$T_{1,20}$ = 340.7	$T_{1,20}$ = 340.7
manipulated variable	Q_{R1}/F_1	Q_{R1}/F_1	Q_{R1}/F_1	Q_{R2}	FQ_{R2} ratio	RR_1
transmitter range (K)	250−450	250−450	250−450	250−450	250−450	250−450
controlled output range (W)	0−7.77 × 10^6	0−0.39 × 10^6	0−0.39 × 10^6	0−0.28 × 10^6	0−1.0 × 10^6	0−4.32 × 10^6
Kc	2.78	14.27	14.27	25.6	25.6	15.9
τ_1 (min)	11.88	5.28	5.28	2.64	2.64	5.28
	TC2	TC2	TC2	TC2	TC2	TC2
controlled variable	$T_{2,9}$ = 417.7	$T_{2,9}$ = 417.7	$T_{2,9}$ = 426.9	$T_{2,9}$ = 427	$T_{2,9}$ = 426.9	$T_{2,9}$ = 426.9
manipulated variable	Q_{R2}	Q_{R2}	Q_{R2}	RR_2	RR_2	RR_2
transmitter range (K)	250−600	250−600	250−600	250−600	250−600	250−600
controlled output range (W)	0−0.81 × 10^6	0−0.28 × 10^6	0−0.28 × 10^6	0−2.16 × 10^6	0−2.16 × 10^6	0−2.6 × 10^6
Kc	0.5	3.62	3.62	3.365	3.36	3.81
τ_1 ((min)	3	9.24	9.24	11.88	11.88	9.24
					CC1	
controlled variable					x(DMC)	
manipulated variable					$T_{1,20}$	
transmitter range					0−2.00	
controlled output range (W)					250−450	
Kc					1	
τ_1 (min)					20	

LP-HP process for this alternative control structure FHICS1 appears to be the logical choice; however, the temperatures are affected much less by the reflux ratio than by vapor boil-up. Thus, the ability to maintain the bottom products of the LP column is not as effective as expected.

Figure 18a shows the performance of the structure FHICS1 for 20% step changes in the feed flowrate disturbances. As the feed flowrate increases at t = 0.2 h, the two bottom flowrates (B_1 and B_2) and two distillate flowrates (D_1 and D_2) all increase. The ninth tray temperature of the HP column increases from 461 to 467 K, and it returns to its set point in 1 h with regulation by the temperature controller. This loop is relatively fast due to the short integral time (11.88 min).

The largest transient deviation of XB_1(MeOH) decreased from 0.995 to 0.982 wt % for the +20% feed flowrate, and the largest transient deviation of XB_2(DMC) decreased smoothly from 0.995 to 0.992 wt % for the +20% feed flowrate disturbance. Such feed flowrate increases make the temperature in the stripping section decrease, enabling a greater amount of light components to escape from the bottom.

The effectiveness of FHICS1 for 20% step changes in feed composition disturbances are illustrated in Figure 16b, their fluctuation trend is similar except that the transient deviation in Figure 18a is slightly smaller. Moreover, the new steady-state values of FHICS1 deviates from their previous steady-state values. Consequently, a feed forward ratio control strategy is proposed to improve the dynamic performance of FHICS1, where the reboiler heat input Q_{R2} of the HP column is proportional to the feed flowrate F. Figure 20 depicts this improved control strategy.

3.3.2. Second Control Structure FHICS2. A multiplier block with two input signals was added to the FHICS1: one input is the feed flowrate F and the other is the Q_{R2}-to-F ratio. The steady-state value of the ratio is 12.63 (GJ/h)/20.90 (kmol/h) = 0.6043. The ultimate gains and periods of the two temperature controllers were obtained by relay-feedback

https://doi.org/10.1021/acsomega.3c00656
ACS Omega 2023, 8, 20450−20470

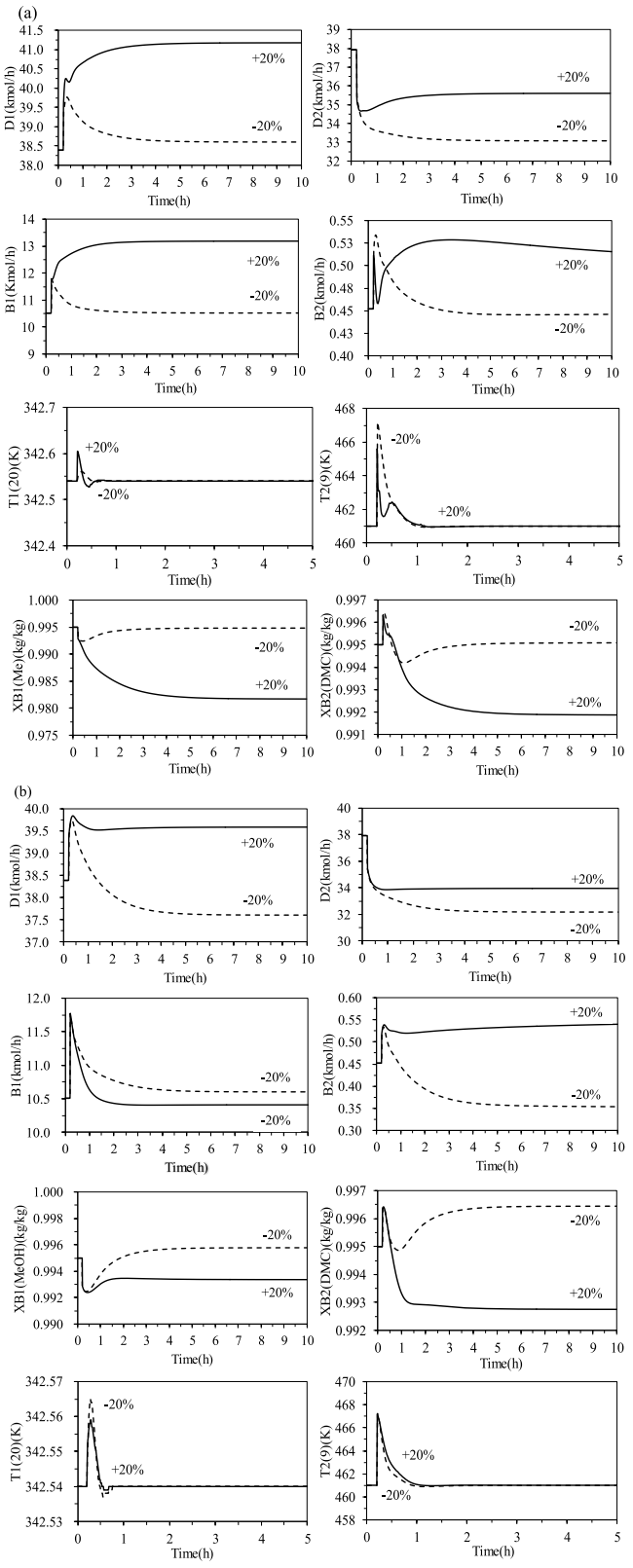

Figure 18. Dynamic responses forFHICS1: (a) 20% feed flowrate disturbances and (b) 20% feed composition disturbances.

tests; the tuning parameters were found to remain almost unchanged for FHICS2 (Figure 19).

The effectiveness of this structure is illustrated by comparing the dynamic response with that of FHICS1. Figure 20a,b compares the responses of the two systems for the +20%

Table 5. Comparison of Design Variables and TAC for Different Separation Sequences

	HPC-LPC		LPC-HPC	
	HPC	LPC	LPC	HPC
Nstage	32	26	24	11
feed stage	10	7	6	7
D (m)	0.53	0.63	0.67	0.48
Q_R (kW)	785	620	735	690
Q_C (kW)	701	1000	−960	−577
A_C (m^2)	7.3288	32.2683	10.0455	6.0344
A_R (m^2)	15.8025	19.0183	14.8034	13.8984
shell (10^6\$)	0.1070	0.1072	0.1076	0.0364
HX (10^6\$)	0.0705	0.1193	0.0747	0.0638
energy (10^6\$/y)	0.1160	0.0926	0.109	0.1023
capital (10^6\$)	0.1770	0.2264	0.1824	0.1003
TAC (10^6\$/y)	0.1760	0.1680	0.1698	0.1358
total capital (10^6\$)	0.4034		0.2827	
total energy (10^6\$/y)	0.2086		0.2113	
TAC (10^6\$/y)	0.3440		0.3056	

disturbances in the feed flowrate and feed composition; the solid lines represent FHICS2 and the dashed lines represent FHICS1. According to the general case, when the Q_R/F controller control structure is applied, the transient deviation should be relatively smaller than when it is not applied. Instead, the results shown in Figure 20a indicate that the disturbances are larger than those when unused. There are large transient dips in X_{B1}(MeOH) and X_{B2}(DMC). The largest transient deviation of X_{B1}(MeOH) decreased from 0.995 to 0.975 wt %, and the largest transient deviation of X_{B2}(DMC) decreased from 0.995 to 0.984 wt % for the +20% feed flowrate disturbance. These results are attributed to the rapid decrease in Q_{R2} caused by the ratio controller "Q_R/F", which allowed more of the volatile component MeOH to escape from the bottom of the HP column. The purity of the DMC product in the HP column goes through a large transient (decrease to 0.987 wt) because the top pressure of the HP column is uncontrolled but floating with the operation status and the bottom temperature of the HP column is fixed. The reboiler input increases with increasing feed flowrate; in turn, this results in a rise in HP column operating pressure, then a greater concentration of MeOH formed on the sensitive plate and gathered at the tops of the pressured column.

According to the distillation theory, a higher DMC concentration in the feed results in a higher overhead pressure of LP column; therefore, a higher MeOH concentration will be produced on the sensitive plate and a higher concentration of the light component will come out from the bottoms that is the reason why a slightly larger transient decrease occurs in X_{B1}(MeOH) and X_{B2}(DMC) for FHICS2 than FHICS1.

Simulation results show that a full integrated system cannot effectively maintain the product concentration well. Because the HP column pressure is not controlled but floats, the energy needed in the condenser/reboiler alters with the feed flowrate and feed composition, then higher HP column operating pressure is produced and larger condenser/reboiler temperature difference is achieved to ensure the LP column reboiler heat input. If the HP column temperature controller setting is fixed, a lower DMC concentration on the sensitive plate is achieved, and more MeOH will escape from the base, so it is not feasible for the fully heat-integrated PSD process to

https://doi.org/10.1021/acsomega.3c00656
ACS Omega 2023, 8, 20450−20470

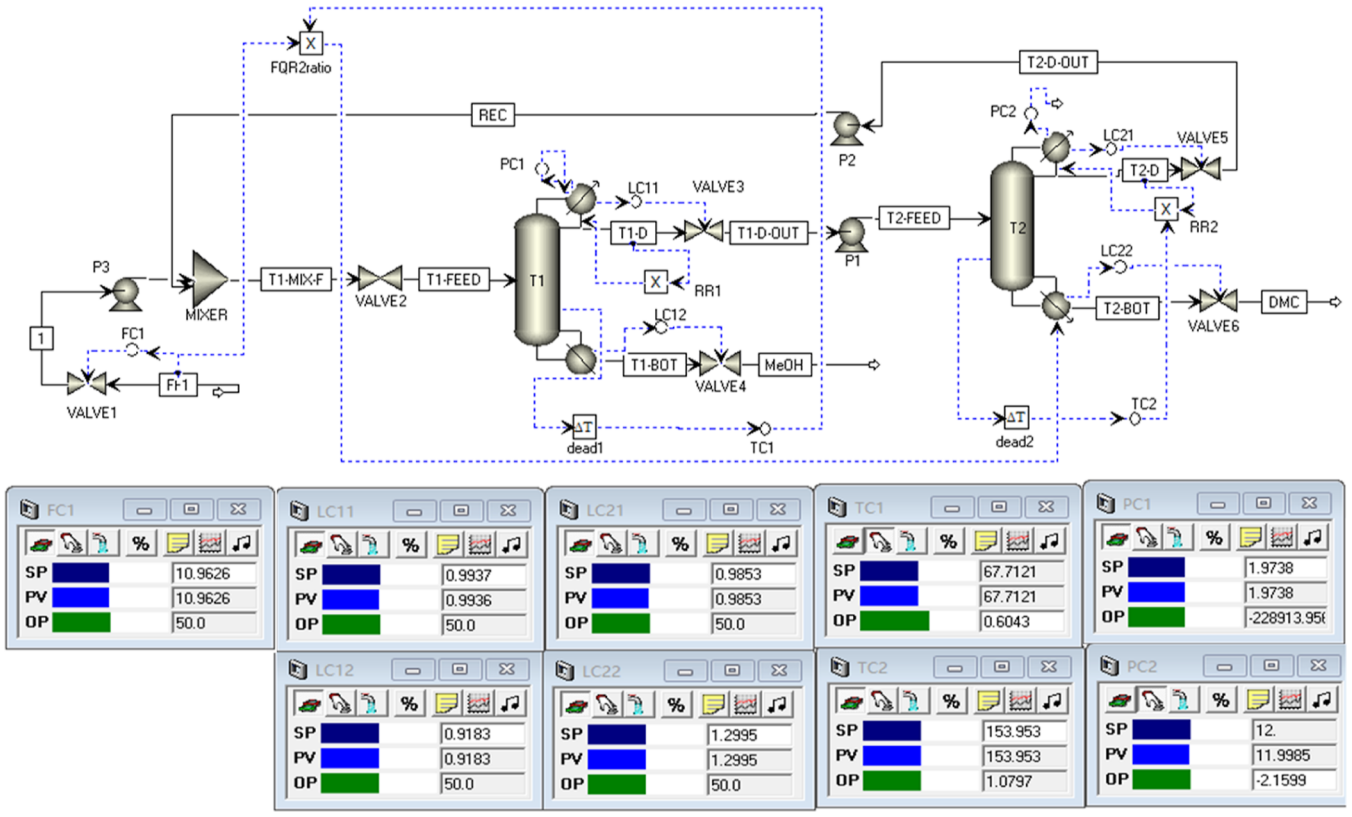

Figure 19. Control structure with full heat integration-FHICS2.

maintain the sensitive plate temperature. Solving this problem requires a PCTC.

3.3.3. Pressure-Compensated Temperature Control. PCTC has been studied previously. A partially heat-integration system with PCTC for THF/water separation has been discussed by Luyben.[34] A full heat-integrated system with PCTC for separating methylal/methanol was proposed by Yu.[35] Based on these simulation results, a fully heat-integrated PSD system with PCTC appears to perform well. Prior to setting up PCTC, the vapor−liquid equilibrium data need to be calculated. After the data were acquired from the steady-state simulation, the bubble-point temperature of the liquids (in stage 9 of the HP column) was plotted against the pressure for this mixture (in the range of 10−15 bar); the plot is shown in Figure 21. Using the following equation, the pressure-compensated temperature was calculated based on the fitted data with a straight line with a slope of 3.3486

$$T_{PC} = T_{2,9}\text{-}3.3486 \times (P\text{-}12)$$

where $T_{2,9}$ is the stage 9 temperature of the HP column, P is the top pressure of the HP column, and T_{PC} is the process variable signal fed into controller TC2 (Figure 23).

A PCTC is implemented using "flowsheet equations" function in Aspen Dynamics (Figure 22), which is compiled by the third equation.

Figure 23 illustrates the PCTC scheme, reflux ratio RR_2 is varied with the pressure-compensated temperature. A composition controller that detects the MeOH concentration in the bottom of LP column and a "dead time" element with a dead time of 3 min were added in the control loop. The dynamic effectiveness is verified by the same disturbances in the feed flowrate and feed composition, which are illustrated in Figure 24a,b, respectively.

Table 4 shows the temperature controller tuning parameters for each control structure.

Stable column operation can be achieved for 20% throughput changes. Two product purities, X_{B1} (MeOH) and X_{B2}(DMC), both return to the desired specifications 99.5 wt% in about 3 h. In particular, this proposed composition/temperature (CC/TC) cascade control structure has an excellent dynamic performance for a 20% decrease in feed flowrate, which is attributable to the two reflux ratios, RR_1 and RR_2, not being held constant but instead allowed to vary with TC1 and T_{PC}, respectively. Furthermore, as the total feed flowrate increases, the ascending velocity of vapor decreases, leading to a decrease in the sensitive plate temperatures T_{20} (in LP column) and T_9 (in HP column).

According to analysis, for the LP column, the CC/TC cascade control was used, sensitive plate temperature T_{20} in the LP column increased while the feed flow decreased, which results in an increase in RR_1; thus, X_{B1}(MeOH) will return to the desired values after fluctuation adjustment.

For the HP column, the distillate flowrate D_1, that is, the feed flowrate into the HP column decreases as the reflux ratio RR_1 decreases, which resulted in a reduction in both the reboiler heat input Q_{R1} and condenser heat removal Q_{C2}. Particularly, this PCTC with a CC/TC cascade control scheme accelerates signaling between the two columns. Thus, it took less time for X_{B2}(DMC) to return to the initial values after fluctuation adjustments, even in the face of 20% feed flowrate and feed composition disturbances.

https://doi.org/10.1021/acsomega.3c00656
ACS Omega 2023, 8, 20450−20470

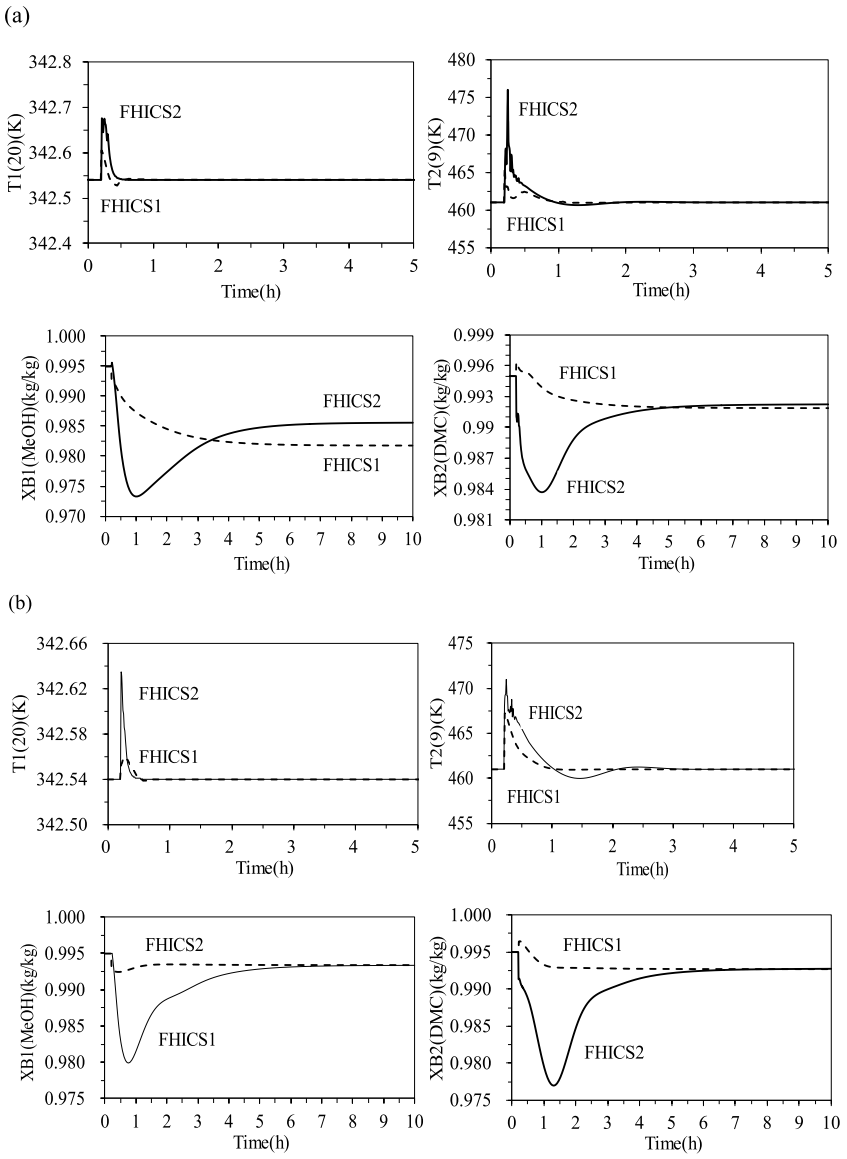

Figure 20. FHICS2 vs FHICS1: (a) −20% feed flowrate disturbances and (b) −20% feed composition disturbances.

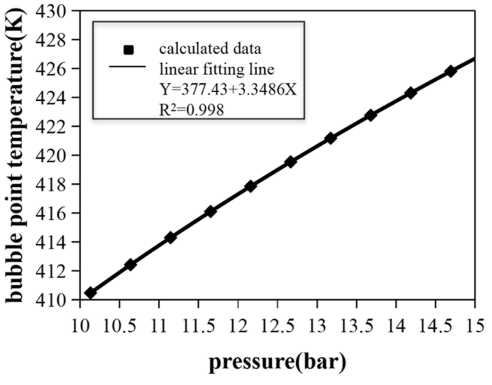

Figure 21. Effect of the system pressure on the bubble-point temperature.

4. RESULTS AND DISCUSSION

4.1. Comparison of Different PSD Separation Sequence. Among the numerous literature studies, two separation sequences, LPC-HPC and HPC-LPC, are commonly reported to achieve azeotrope separation. Based on our previously published case report, a pressurized-atmospheric process for separation of DMC/MeOH azeotrope without heat integration[15] is shown in Figure 25a, the atmospheric-pressurized process proposed in this paper is shown in Figure 25b, and the optimal design parameters obtained by minimum TAC are shown in Figure 26. The comparison of the design variables and minimum TAC for two separation sequences are presented in Table 5. It is evident that the energy cost of the LPC-HPC sequence is 0.2113*e^6 \$/y, only 1.29% more than HPC-LPC sequences, while the TAC of the LPC-HPC sequence is 0.3056*e^6 \$/y, with a reduction of 11.16% compared to HPC-LPC sequences. Considered together, the LPC-HPC process is favored over the LPC-HPC process in energy-saving potential.

Consequently, in the present study, this energy-efficient atmospheric-pressurized process was proposed for separating the DMC/MeOH azeotrope.

4.2. Economy of the Process with No, Partial, and Full Heat Integration. The economic performance of the atmospheric-pressurized process for DMC/MeOH separation

https://doi.org/10.1021/acsomega.3c00656
ACS Omega 2023, 8, 20450−20470

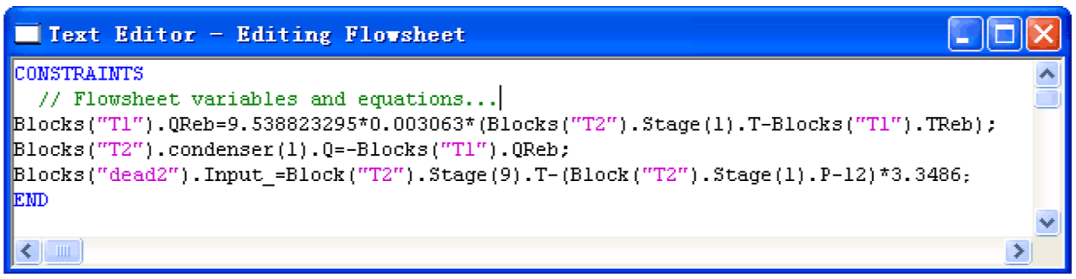

Figure 22. Flowsheet equations with the pressure-compensated temperature.

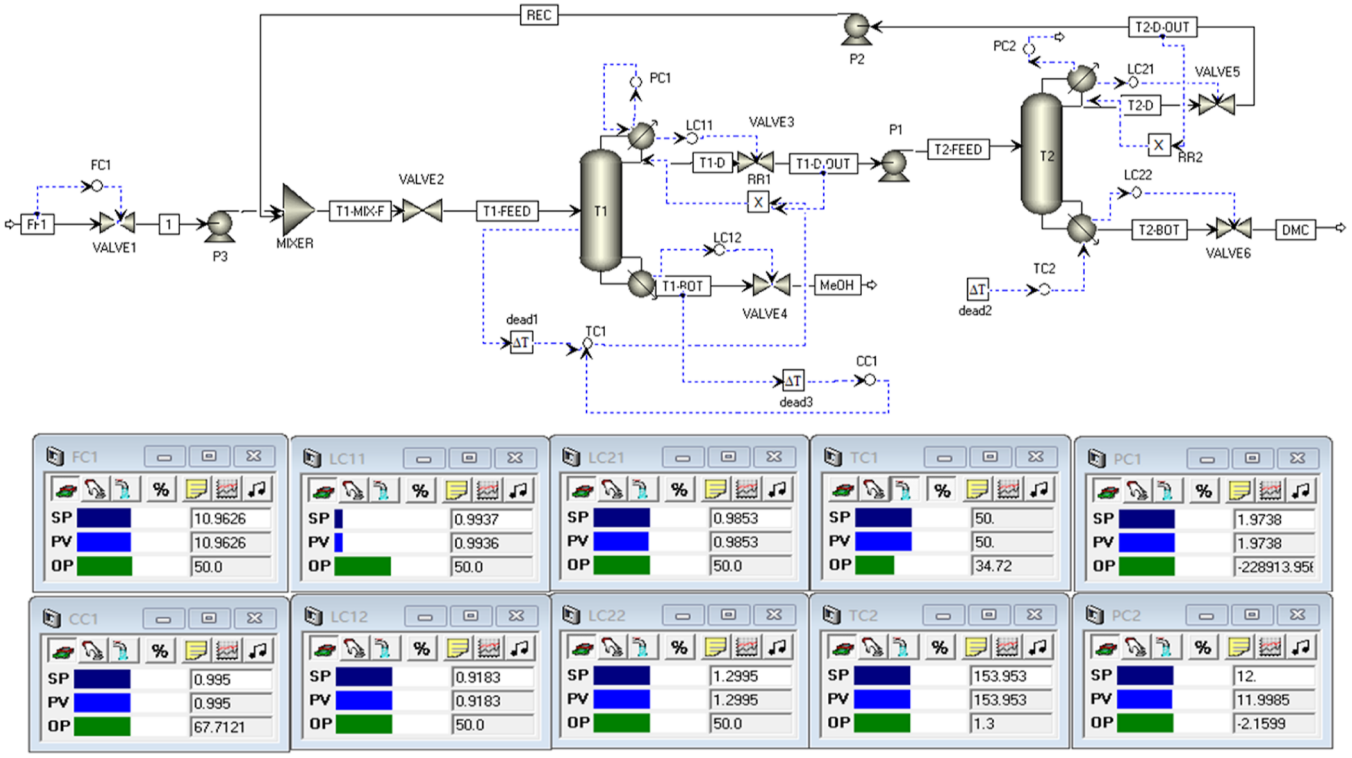

Figure 23. PCTC structure with CC/TC cascade control.

with no, partial, and full heat integration is shown in Table 2, the TAC with no, partial, and full heat integration are $0.3056*10^6$ \$/y, $0.1950*10^6$ \$/y, and $0.1858*10^6$ \$/y, respectively, and the separation via full heat integration can cut the TAC by as much as 39.2% and that partial heat integration can reduce the TAC by as much as 36.2%. Evidently, the full heat integration process was more energy efficient.

4.3. Controllability of the Process with No, Partial, and Full Heat Integration. The dynamic controllability of the process with no, partial, and full heat integration were evaluated by introducing feed flowrates and composition disturbances. In the face of 20% feed disturbances, good dynamic performance has been demonstrated for non-heat-integrated systems when faced with 20% feed disturbances: the transient deviation of X_{B1}(MeOH) and X_{B2}(DMC) is approximately 2200 and 1 ppm for large feed flowrate disturbances; during the transient, the product purities X_{B1}(DMC) and X_{B2}(MeOH) are very close to their desired values.

For the partially heat-integrated process: in PHICS1, a feed-forward ratio control structure "Q_{aux}/F_1" was added to improve dynamic performance, feed interferences were well handled with stable regulatory control achieved; nonetheless, the largest transient deviation of X_{B1}(MeOH) decreased from 0.995 to 0.993 wt % for +20% feed flowrate disturbance; while the transient deviation in X_{B1}(MeOH) is very small for feed composition disturbances, the largest transient deviation of X_{B2}(DMC) decreased from 0.995 to 0.990 wt % for +20% feed flowrate disturbance and the largest transient deviation of X_{B2}(DMC) decreased from 0.995 to 0.992 wt % for +20% feed composition disturbance. This reveals that the system was able to respond well to these disturbances except for X_{B2} (DMC), particularly, it took more time for X_{B2}(DMC) than X_{B1}(MeOH) to regain stability after deviation. In PHICS2, a ratio block "Q_{Rtot}/F" and summation block were used, which resulted in control performances similar to those of non-heat integration; slightly large deviations in X_{B2}(DMC) were displayed for disturbances in both feed flowrate and feed composition: the largest transient deviation of X_{B2}(DMC) decreased from 0.995 to 0.991 wt % for the +20% feed flowrate disturbance and the largest transient deviation of X_{B2}(DMC) decreased from 0.995 to 0.993 wt % for the +20% feed composition disturbance.

https://doi.org/10.1021/acsomega.3c00656
ACS Omega 2023, 8, 20450−20470

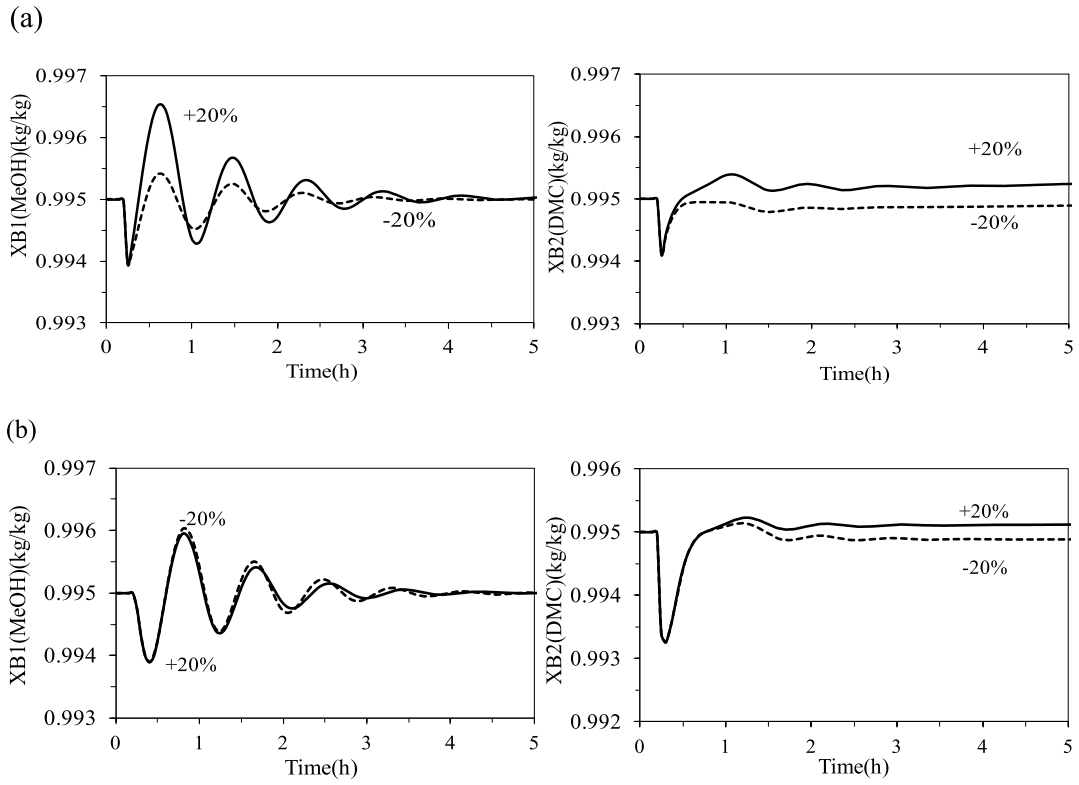

Figure 24. Dynamic responses for the PCTC structure: (a) 20% feed flowrate disturbances and (b) 20% feed composition disturbances.

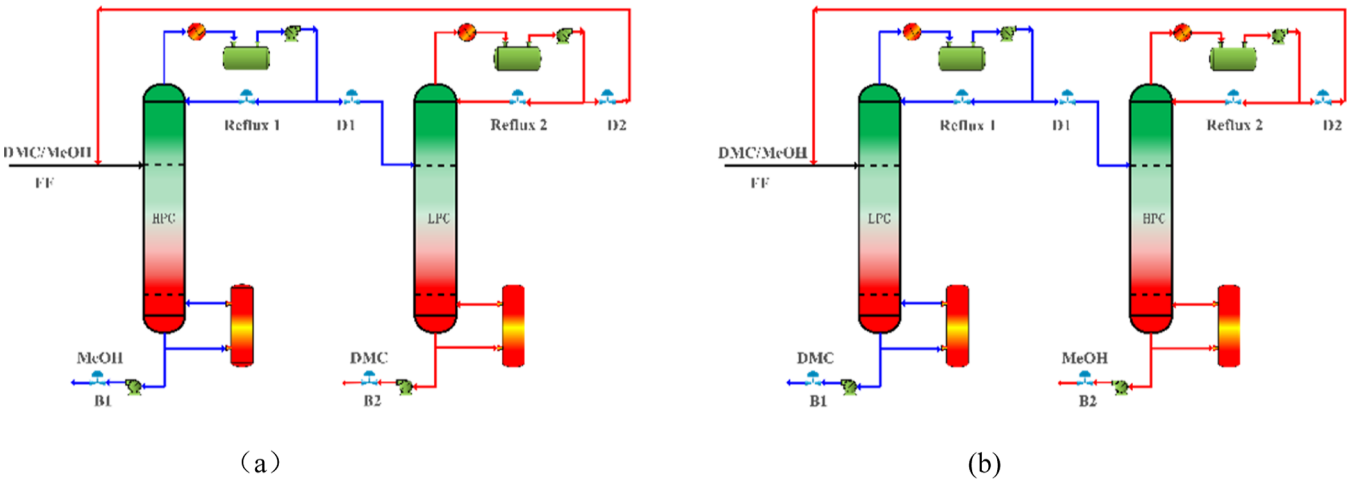

Figure 25. Two separation sequences: (a) HPC-HPC and (b) LPC-HPC.

For the fully heat-integrated process, critical dynamic penalties have been demonstrated for FHICS1: the largest transient deviation of XB_1(MeOH) decreased from 0.995 to 0.982 wt % for +20% feed flowrate disturbance and the largest transient deviation of XB_2(DMC) decreased smoothly from 0.995 to 0.992 wt % for +20% feed flowrate disturbance. The fluctuation of the feed composition was similar to those observed for feed flow disturbances. Similar dynamic penalties are also demonstrated for FHICS2.

A PCTC structure with CC/TC cascade control can reduce oscillations and return to a new steady state faster than FHICS1 and FHICS2. Especially, it could maintain the product purity accurately.

5. CONCLUSIONS

An atmospheric-pressurized process for DMC/MeOH separation with a heat-integrated PSD was presented in this paper. The economic performance of atmospheric-pressurized and pressurized-atmospheric sequence was compared. It was proved that the former was more energy efficient. Different types of heat-integrated systems were investigated to save costs, including no, partial, and full heat integration. Several optimized configurations were proposed using the developed optimization method with the commercial software Aspen Plus. It was revealed that the fully heat-integrated process is more competitive than the other processes from an economical viewpoint.

https://doi.org/10.1021/acsomega.3c00656
ACS Omega 2023, 8, 20450−20470

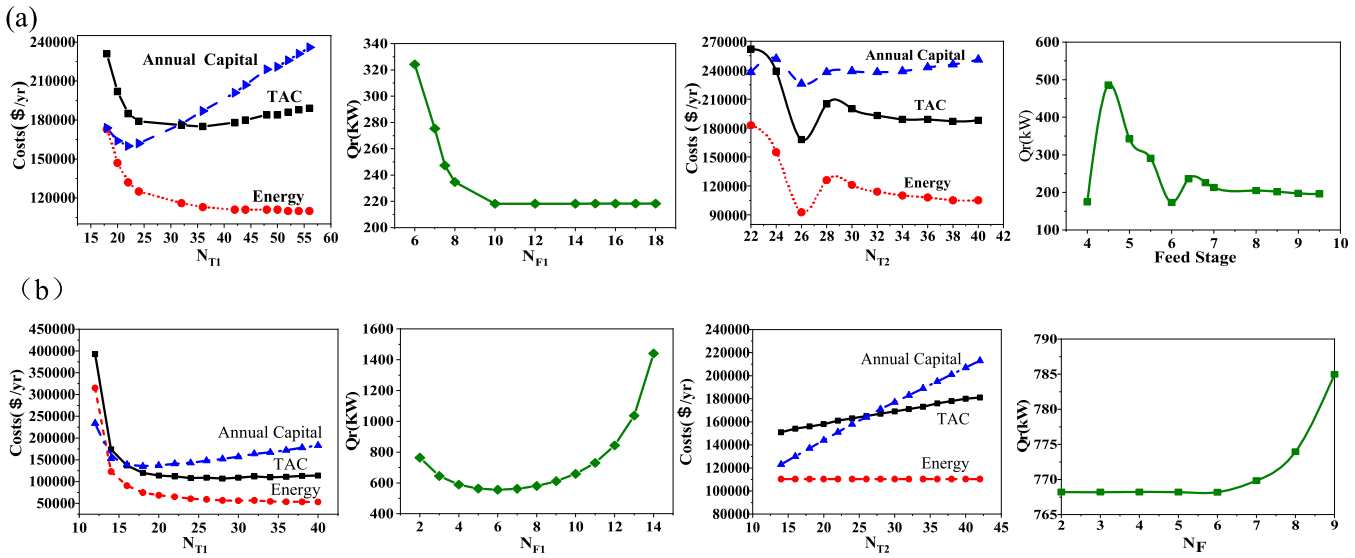

Figure 26. Effects of operation parameters on TAC and Qr: (a) HPC-LPC process and (b) LPC-HPC process.

Several control schemes for this process were explored, ranging from no integration to full heat integration. Critical dynamic penalties were demonstrated for both full and partial heat integration, while partial heat integration provides much more robust control. Their respective dynamic performance was compared and demonstrated in detail. These proposed control structures with partial and full heat integration could not maintain their product specifications very efficiently for large feed disturbances. A CC/TC-cascaded PCTC structure could precisely maintain the product concentration effectively for the fully heat-integrated PSD process. This paper updates our previous works and the results demonstrate that the system with full integration can realize stronger robustness.

These findings of our study provide a novel energy-saving pathway and provide some guiding significance for the design and control of DMC/MeOH azeotrope separation in the industrialization process.

■ ASSOCIATED CONTENT

Supporting Information

The Supporting Information is available free of charge at https://pubs.acs.org/doi/10.1021/acsomega.3c00656.

Economic modeling for the dimethyl carbonate/methanol separation process (PDF)

■ AUTHOR INFORMATION

Corresponding Authors

Wei-Zhou Jiao − *Shanxi Province Key Laboratory of Higee-Oriented Chemical Engineering, North University of China, Taiyuan 030051 Shanxi, China*; orcid.org/0000-0003-3378-6743; Email: jwz0306@126.com

Wei Wei − *Low Carbon Energy Conversion Technology Research Center, Shanghai Advanced Research Institute, Chinese Academy of Science, Shanghai 201203, P. R. China*; orcid.org/0000-0003-0043-1583; Email: weiwei@sari.ac.cn

Authors

Hong-mei Wei − *Department of Mechanical Engineering, North University of China, Taiyuan 030051 Shanxi, China*; orcid.org/0000-0002-1314-7752

Fu-jie Wang − *Department of Mechanical Engineering, North University of China, Taiyuan 030051 Shanxi, China*

Hong-wei Yan − *Department of Mechanical Engineering, North University of China, Taiyuan 030051 Shanxi, China*

Complete contact information is available at: https://pubs.acs.org/10.1021/acsomega.3c00656

Notes

The authors declare no competing financial interest.

■ ACKNOWLEDGMENTS

This work was supported by Science Foundation of North University of China (no: 110246); Foundation of Shanxi Province Key Laboratory of Higee-Oriented Chemical Engineering (no: CZL2020-06); Fundamental Research Program of Shanxi Province (no: 20210302123054); the Fundamental Research Program of Shanxi Province (no: 20210302123038); the Special project of scientific and technological cooperation and exchange in Shanxi Province (no: 202104041101001); and Research Project Supported by Shanxi Scholarship Council of China (no: 2020-110).

■ NOMENCLATURE

TAC ($/year)	total annual cost
N_T	total number of column trays
N_F	feed tray location of a column
D_n (kmol/s)	distillate flowrate of the *n*th column
B_n (kmol/s)	bottom flowrate of the *n*th column
RR	reflux ratio
D (m)	column diameter
Q_R (GJ/h)	reboiler heat input
Q_C (GJ/h)	condenser heat removal
A_C (m^2)	reboiler heat-transfer areas
A_R (m^2)	condenser heat-transfer areas
shell ($10^6$$)	capital cost of the shell
HX ($10^6$$)	the heat exchanger cost
energy ($10^6$$/y)	the cost of energy
CC/TC	cascade composition/temperature control structure
CS*n*	the *n*th control strategy
Q_R/F	reboiler heat input-to-feed ratio

https://doi.org/10.1021/acsomega.3c00656
ACS Omega 2023, 8, 20450−20470

X_{B1} (kg/kg)	DMC purity at the bottom of HP column
X_{B2} (kg/kg)	methanol purity at the bottom of LP column
$T_{n,m}$ (K)	temperature of try m in column n
T_{PC} (K)	pressure-compensated temperature
NHICS	non-heat-integrated control structure
PHICS	partially heat-integrated control structure
FHICS	fully heat-integrated control structure

REFERENCES

(1) Delledonne, D.; Rivetti, F.; Romano, U. Developments in the production and application of dimethylcarbonate. *Appl. Catal., A* **2001**, *221*, 241−251.

(2) Jiang, Z. Y.; Wang, Y. Preparation of dimethyl carbonate through transesterification in a catalytic distillation column. *Chem. Eng.* **2001**, *29*, 29−61.

(3) Bayer, A. G. Process for the preparation of carbonic esters. European Patent. EP 0061672 A1, 1982.

(4) Ryu, J. Y. Process for making dialkyl carbonates. U.S. Patent 5,902,894 A, 1999.

(5) Saleh, R. Y.; Michaelson, R. C.; Suciu, E. N.; Kuhlmann, B. Process for manufacturing dialkyl carbonate from urea and alcohol. U.S. Patent 5,565,603 A, 1996.

(6) Sun, J.; Yang, B.; Lin, H. A Semi-continuous Process for the Synthesis of Methyl Carbamate from Urea and Methanol. *Chem. Eng. Technol.* **2004**, *27*, 435−439.

(7) Phimister, J.; Seider, W. Semicontinuous, Pressure-Swing Distillation. *Ind. Eng. Chem. Res.* **2000**, *39*, 122−130.

(8) Luyben, W. L. Pressure-Swing Distillation for Minimum- and Maximum-Boiling Homogeneous Azeotropes. *Ind. Eng. Chem. Res.* **2012**, *51*, 10881−10886.

(9) Zhang, Z.; Zhang, Q.; Li, G.; Liu, M.; Gao, J. Design and control of methyl acetate-methanol separation via heat-integrated pressure-swing distillation. *Chin. J. Chem. Eng.* **2016**, *24*, 1584−1599.

(10) Liang, S.; Cao, Y.; Liu, X.; Li, X.; Zhao, Y.; Wang, Y.; Wang, Y. Insight into pressure-swing distillation from azeotropic phenomenon to dynamic control. *Chem. Eng. Res. Des.* **2017**, *117*, 318−335.

(11) Zhu, Z.; Xu, D.; Wang, Y.; Geng, X.; Wang, Y. Effect of multi-recycle streams on triple-column pressure-swing distillation optimization. *Chem. Eng. Res. Des.* **2017**, *127*, 215−222.

(12) Yang, A.; Shen, W.; Wei, S. a.; Dong, L.; Li, J.; Gerbaud, V. Design and Control of Pressure-Swing Distillation for Separating Ternary Systems with Three Binary Minimum Azeotropes. *AIChE J.* **2019**, *65*, 1281−1293.

(13) Salman, M.; Javed, N.; Liu, X.; He, M. Azeotrope separation of ethyl propionate and ethanol by extractive distillation and pressure swing distillation method. *Sep. Purif. Technol.* **2023**, *311*, 123361.

(14) Li, C.; Zhang, X.; Zhang, s.; Xu, Q. Vapor-Liquid Equilibria and Process Simulation for Separation of Dimethyl Carbonate and Methanol Azeotropic System. *Chin. J. Process Eng.* **2003**, 453−458.

(15) Zhang, J.; Wang, F.; Peng, W.; Xiao, F.; Wei, W.; Sun, Y. Process simulation for separation of dimethyl carbonate and methanol through atmospheric-pressurized rectification. *Petrochem. Technol.* **2010**, *39*, 646−650.

(16) Wei, H.-M.; Wang, F.; Zhang, J.-L.; Liao, B.; Zhao, N.; Xiao, F.-k.; Wei, W.; Sun, Y.-H. Design and Control of Dimethyl Carbonate−Methanol Separation via Pressure-Swing Distillation. *Ind. Eng. Chem. Res.* **2013**, *52*, 11463−11478.

(17) Huang, Z.; Lin, Y.; Wang, X.; Ye, C.; Li, L. Optimization and control of a reactive distillation process for the synthesis of dimethyl carbonate. *Chin. J. Chem. Eng.* **2017**, *25*, 1079−1090.

(18) An, R.; Chen, S.; Li, H.; Li, X.; Jin, Y.; Li, C.; An, W.; Liu, R. Energy-saving reactive pressure-swing distillation process for separation of methanol-dimethyl carbonate azeotrope via reacting with propylene oxide. *Sep. Purif. Technol.* **2022**, *292*, 120889.

(19) Huang, K.; Shan, L.; Zhu, Q.; Qian, J. Adding rectifying/stripping section type heat integration to a pressure-swing distillation (PSD) process. *Appl. Therm. Eng.* **2008**, *28*, 923−932.

(20) Li, R.; Ye, Q.; Suo, X.; Dai, X.; Yu, H. Heat-Integrated Pressure-Swing Distillation Process for Separation of a Maximum-Boiling Azeotrope Ethylenediamine/Water. *Chem. Eng. Res. Des.* **2016**, *105*, 1−15.

(21) Modla, G.; Lang, P. Feasibility of new pressure swing batch distillation methods. *Chem. Eng. Sci.* **2008**, *63*, 2856−2874.

(22) Varbanov, P.; Klein, A.; Repke, J. U.; Wozny, G. Minimising the startup duration for mass- and heat-integrated two-column distillation systems: A conceptual approach. *Chem. Eng. Process.* **2008**, *47*, 1456−1469.

(23) Wang, Y.; Ma, K.; Yu, M.; Dai, Y.; Yuan, R.; Zhu, Z.; Gao, J. An improvement scheme for pressure-swing distillation with and without heat integration through an intermediate connection to achieve energy savings. *Comput. Chem. Eng.* **2018**, *119*, 439−449.

(24) Zhu, Z.; Xu, D.; Jia, H.; Zhao, Y.; Wang, Y. Heat Integration and Control of a Triple-Column Pressure-Swing Distillation Process. *Ind. Eng. Chem. Res.* **2017**, *56*, 2150−2167.

(25) Abu-Eishah, S. I.; Luyben, W. L. Design and control of a two-column azeotropic distillation system. *Ind. Eng. Chem. Process Des. Dev.* **1985**, *24*, 132−140.

(26) Ding, S. S.; Luyben, W. L. Control of a heat-integrated complex distillation configuration. *Ind. Eng. Chem. Res.* **1990**, *29*, 1240−1249.

(27) Knapp, J. P.; Doherty, M. F. Thermal integration of homogeneous azeotropic distillation sequences. *AIChE J.* **1990**, *36*, 969−984.

(28) Shen, Y.; Zhao, F.; Qiu, X.; Zhang, H.; Yao, D.; Wang, S.; Zhu, Z.; Yang, J.; Cui, P.; Wang, Y.; et al. Economic, Thermodynamic, and Environmental Analysis and Comparison of the Synthesis Process of Butyl Acetate. *Ind. Eng. Chem. Res.* **2020**, *59*, 21869−21881.

(29) Suo, X.; Ye, Q.; Li, R.; Dai, X.; Yu, H. The partial heat-integrated pressure-swing reactive distillation process for transesterification of methyl acetate with isopropanol. *Chem. Eng. Process.* **2016**, *107*, 42−57.

(30) Yu, A.; Ye, Q.; Li, J.; Li, X.; Wang, Y.; Rui, Q. Improving the economy and energy efficiency of separating n-propanol/water/tetrahydrofuran via triple-column pressure-swing distillation and azeotropic combining pressure-swing distillation. *Sep. Purif. Technol.* **2023**, *309*, 123023.

(31) Zhu, Z.; Li, S.; Dai, Y.; Yang, X.; Wang, Y.; Gao, J. Control of a pressure-swing distillation process for benzene/isopropanol/water separation with and without heat integration. *Sep. Purif. Technol.* **2020**, *236*, 116311.

(32) Wei, H.-M.; Gao, Q.; Jiao, W.-z.; Wei, W. Dynamic simulation and control of a triple column process for dimethyl carbonate-methanol separation. *Korean J. Chem. Eng.* **2022**, *39*, 3190−3203.

(33) Repke, J.-U.; Klein, A.; Forner, F. Homogeneous azeotropic distillation in an energy- and mass-integrated pressure swing column system. *Comput.-Aided Chem. Eng.* **2004**, *18*, 757−762.

(34) Luyben, W. L. Design and Control of a Fully Heat-Integrated Pressure-Swing Azeotropic Distillation System. *Ind. Eng. Chem. Res.* **2008**, *47*, 2681−2695.

(35) Yu, B.; Wang, Q.; Xu, C. Design and Control of Distillation System for Methylal/Methanol Separation. Part 2: Pressure Swing Distillation with Full Heat Integration. *Ind. Eng. Chem. Res.* **2012**, *51*, 1293−1310.

(36) Shan, B.; Sun, D.; Zheng, Q.; Zhang, F.; Wang, Y.; Zhu, Z. Dynamic control of the pressure-swing distillation process for THF/ethanol/water separation with and without thermal integration. *Sep. Purif. Technol.* **2021**, *268*, 118686.

(37) Shi, T.; Chun, W.; Yang, A.; Jin, S.; Shen, W.; Ren, J.; Gu, J. The process control of the triple-column pressure-swing extractive distillation with partial heat integration. *Sep. Purif. Technol.* **2020**, *238*, 116416.

(38) Zhang, Q.; Liu, M.; Li, W.; Li, C.; Zeng, A. Heat-integrated triple-column pressure-swing distillation process with multi-recycle streams for the separation of ternary azeotropic mixture of acetonitrile/methanol/benzene. *Sep. Purif. Technol.* **2019**, *211*, 40−53.

(39) Zhang, Q.; Peng, J.; Zhang, K. Separation of an azeotropic mixture of dimethyl carbonate and methanol via partial heat

https://doi.org/10.1021/acsomega.3c00656
ACS Omega 2023, 8, 20450−20470

integration pressure swing distillation. *Asia-Pac. J. Chem. Eng.* **2017**, *12*, 50−64.
(40) Luyben, W. L. *Distillation Design and Control Using Aspen TM Simulation*; John Wiley & Sons, Inc., 2013; pp 188−231.
(41) Luyben, W. L. Plantwide Control of an Isopropyl Alcohol Dehydration Process. *AIChE J.* **2006**, *52*, 2290−2296.
(42) Luyben, W. L. Control of a multiunit heterogeneous azeotropic distillation process. *AIChE J.* **2006**, *52*, 623−637.
(43) Luyben, W. L. Control of Ternary Reactive Distillation Columns with and without Chemically Inert Components. *Ind. Eng. Chem. Res.* **2007**, *46*, 5576−5590.
(44) Luyben, W. L. Comparison of Extractive Distillation and Pressure-Swing Distillation for Acetone−Methanol Separation. *Ind. Eng. Chem. Res.* **2008**, *47*, 2696−2707.
(45) Luyben, W. L. Control of the Maximum-Boiling Acetone/Chloroform Azeotropic Distillation System. *Ind. Eng. Chem. Res.* **2008**, *47*, 6140−6149.
(46) Luyben, W. L. Tuning Proportional Integral Derivative Controllers for Integrator/Deadtime Processes. *Ind. Eng. Chem. Res.* **1996**, *35*, 3480−3483.

https://doi.org/10.1021/acsomega.3c00656
ACS Omega 2023, 8, 20450−20470